S.V. Makarov, E.Y. Tiguntseva, P.A. Tonkaev

EXPERIMENTAL METHODS OF NANOPHOTONICS

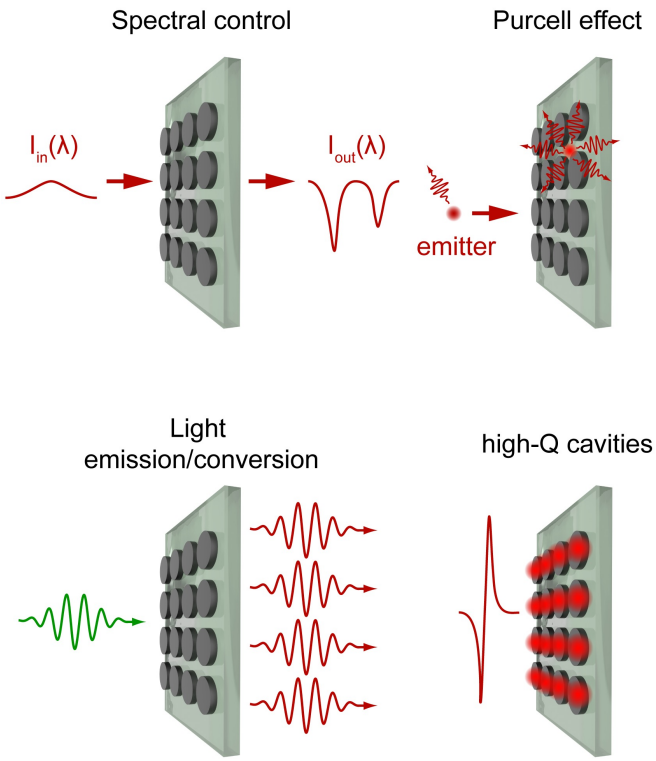

Saint Petersburg
2022

MINISTRY OF EDUCATION AND SCIENCE OF THE RUSSIAN FEDERATION

ITMO UNIVERSITY

S.V. Makarov, E.Y. Tiguntseva, P.A. Tonkaev

EXPERIMENTAL METHODS OF NANOPHOTONICS

STUDY GUIDE

RECOMMENDED FOR USE AT ITMO UNIVERSITY

within the Master's Program 16.04.01 "Technical Physics"

Saint Petersburg
2022

S.V. Makarov, E.Y. Tiguntseva, P.A. Tonkaev, Experimental methods of nanophotonics– St. Petersburg: ITMO University, 2022. – 74 pages.

Reviewers:
Mukhin Ivan Sergeevich, PhD, Researcher at the Chemical and Biological Cluster (fired on December 31, 2021), ITMO University.

Nanophotonics is a rapidly developing field, which aims at tailoring the optical properties of nanomaterials and understanding the optical phenomena arising near or beyond the diffraction limit of light. This course gives insights into contemporary tools and strategies for fabrication and experimental characterization of nanoscale optical devices and structures Being targeted at broad audience intending to work in areas related to nanophotonics, the course is both essential for experimentalists and provides important basic knowledge for theoreticians. Starting from nanofabrication technologies and methods of basic structural characterization, we will proceed to conventional and super-resolution optical imaging, spectroscopy and interferometry. The lectures are accompanied by advanced lab practices, lab projects and seminars on the most important achievements of modern science related to optics and photonics. The study guide is recommended for use in the course "Experimental Methods in Nanophotonics".

CONTENTS

Chapter 1

Laser applications in nanoscience

1.1 History of lasers

The history of Light Amplification by Stimulated Emission of Radiation, or LASER, started 100 years ago, in 1917, when Einstein proposed the concept of stimulated emission. Only 11 years later Ladenburg confirmed stimulated emission in an experiment. The next important step was made in 1940, when population inversion was discovered.

The first laser was implemented in 1960 by Theodore Maiman. It consisted of three main parts: a ruby active medium, two mirrors, which formed an optical cavity, and a flash tube pump. The ruby laser produced light in the visible range of the spectrum, in red colour (694 nm), with a linewidth of 0.53 nm and PCE (Process Cycle Efficiency) about 1-2 % (Fig. 1.1).

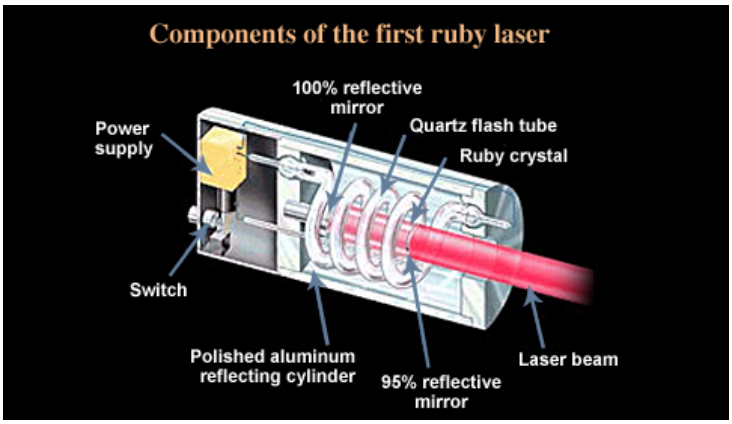

Figure 1.1: Structure of a ruby laser [1].

In 1970, Z.I. Alferov invented the first semiconductor laser, or laser diode. In such lasers, the active laser medium is a p-n junction, and both edges of the active layer have

mirror-like surfaces (Fig. 1.2). Instead of the optical pumping as in a ruby laser, in a semiconductor laser, the active medium is excited by electric current.

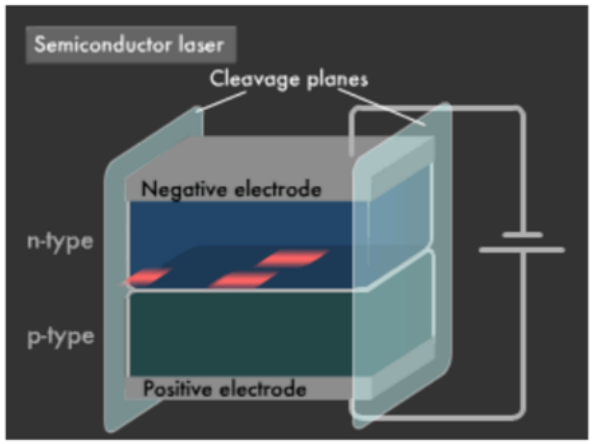

Figure 1.2: Structure of a laser diode [2].

Both ordinary light and laser light are electromagnetic waves, but laser light has three key advantages over ordinary light. Ordinary light is divergent and incoherent, whereas laser light is highly directional and coherent. Directionality is crucial for focusing emission and telecommunication. Ordinary light is a mixture of electromagnetic waves with different wavelengths. Laser light is monochromatic, which is very important for spectroscopy, where the use of a single wavelength and a single frequency is vital. The high monochromaticity of laser light also allows the reduction of chromatic aberration.

1.2 Laser applications

Due to all the unique properties of lasers, they have a great number of applications in various areas of science, industry and medicine. Laser processing can be classified into two groups: conventional laser processing and laser chemical processing. Conventional laser processing is implemented without any changes in the overall chemical composition of the material. Chemical laser processing is characterized by an overall change in the chemical composition of the material or by a activation of a chemical reaction.

Mechanisms of laser beam-matter interaction depend on the laser parameters and the physical and chemical properties of matter. Laser light can excite free electrons in metal or lattice vibrations in insulators. In general, the energy of this excitation dissipates into heat, and as a consequence, a laser beam can be considered as a heat source. Figure 1.3 shows two regimes of laser-material interactions employed in conventional laser processing: below and above the vaporization threshold. Above the vaporization threshold, the regime is characterized by plasma formation and liquid-phase expulsion [3].

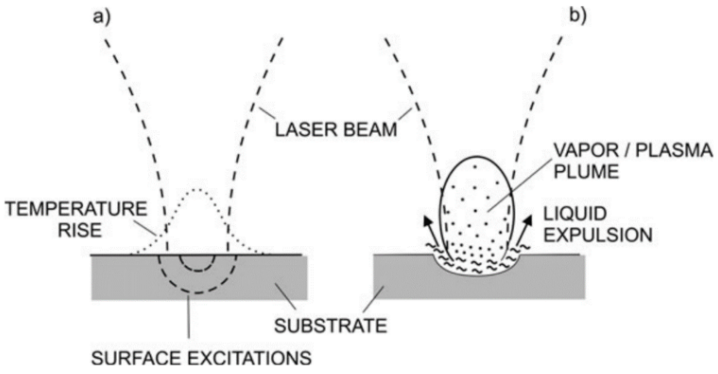

Figure 1.3: Two regimes of laser–material interactions: (a) below vaporization threshold and (b) above vaporization threshold [3].

Due to the above properties of lasers, they have numerous applications in abrasive laser machining: drilling, scribing, cutting, trimming, and shaping. Material is removed as plasma, liquid or vapour, as shown in Fig. 1.3(b). With laser welding and bonding, the material is only melted. Besides, laser-induced annealing, transformation hardening, glazing, re-crystallization can be mentioned. All these applications imply lasers with different intensity ranges.

Besides laser-induced thermal processes, there are non-thermal or photochemical laser processes. Laser radiation can excite molecules, initiating a chemical reaction or speeding it up (Fig. 1.4) [3].

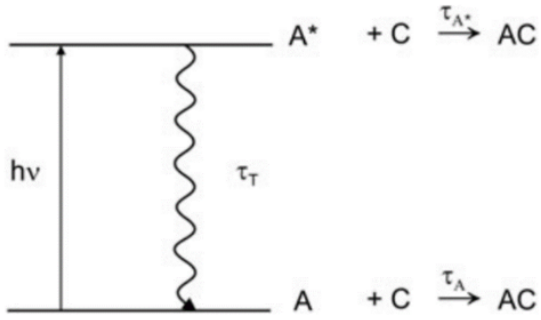

Figure 1.4: A simple model of the competition between a thermal and a photochemical reaction [3].

Lasers play an important role in microscale applications, for example, CD recording and reading. When a laser diode interacts with a phase-change material, it changes its optical properties due to surface heating information on the surface in binary code. Due to the differences in the reflection of irradiated and non-irradiated areas of the phase-change material, the information can be read from the disk.

The main challenge is the development of laser technology in order to decrease the elements' size. Short-wavelength lasers (with a wavelength of about 10 nm), complex

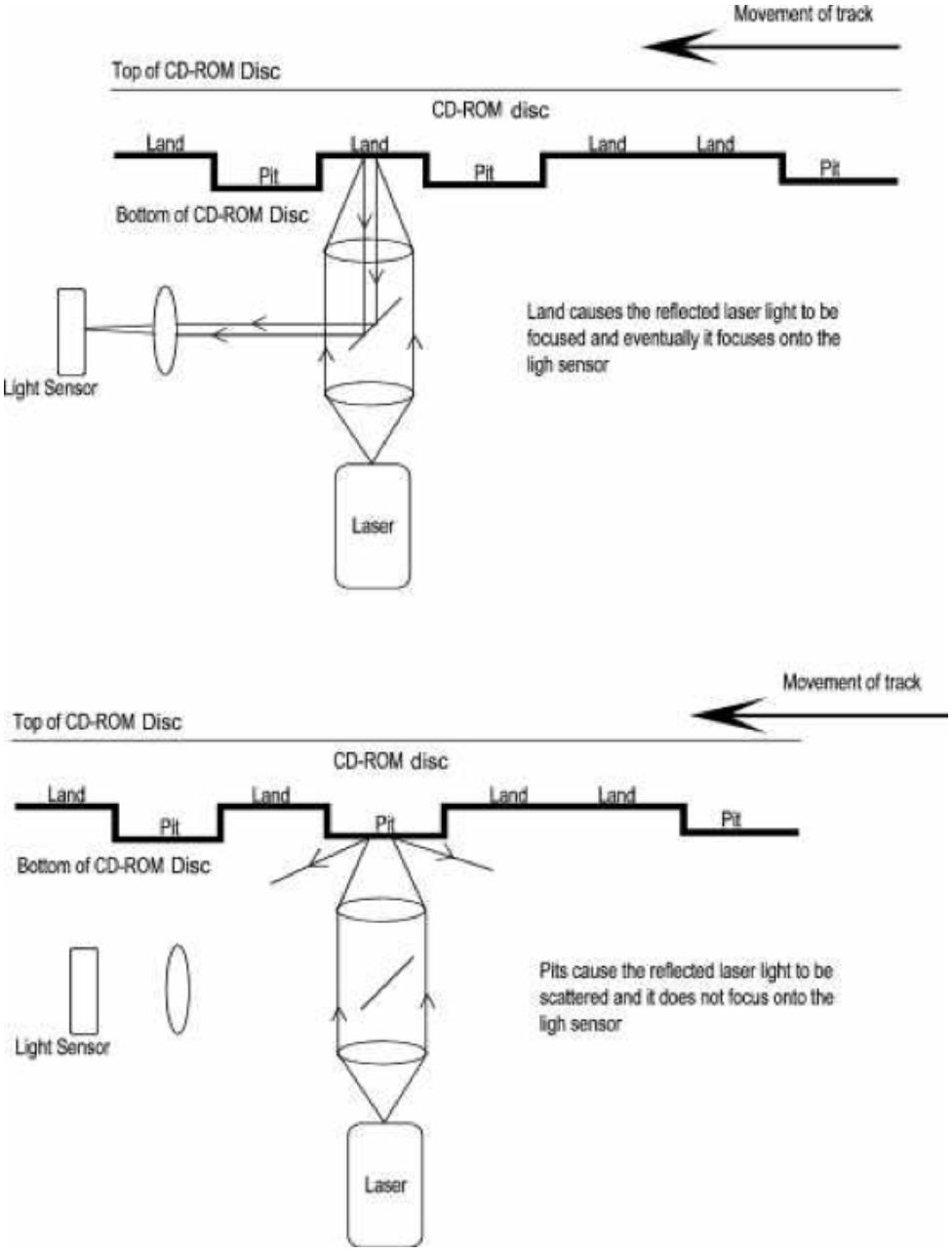

Figure 1.5: Laser recording and reading of a CD [3].

focusing systems and new technological approaches are used for creating transistors approximately 5 nm in size. Fig. 1.6 shows a scheme of extreme ultraviolet lithography with a CO_2 laser and Sn plasma source, operating at a wavelength of 13.5 nm. In this experiment, gas etching after the resist development allowed forming small structures, which are shown in Fig. 1.6.

In addition, metal surfaces can be modified and colorized with a femtosecond laser pulse and carbon dioxide lasers. Plasmonic color (structural colors resulting from resonant

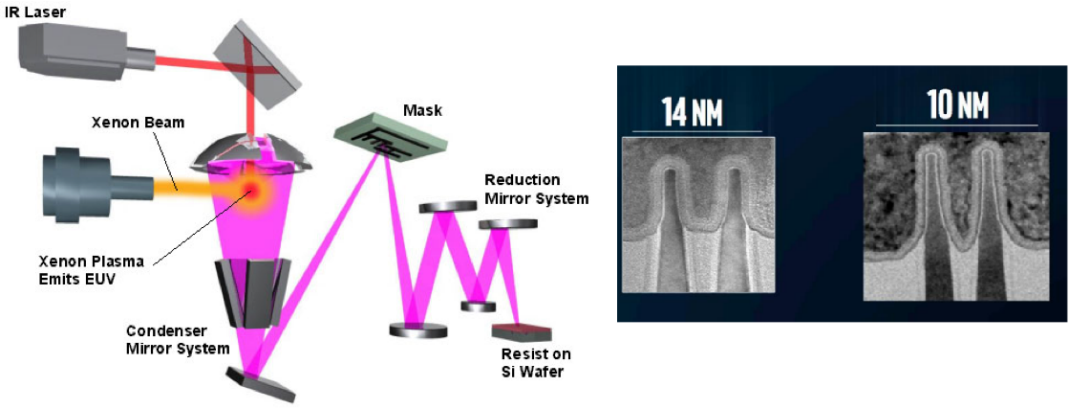

Figure 1.6: Scheme of extreme ultraviolet lithography and examples of structures obtained by extreme ultraviolet lithography [4,5].

interactions between the light and the metallic nanostructures) depend on nanoparticles shape. To obtain such structural coloration, laser-induced heating is used to change the morphology of plasmonic nanostructures due to quick annealing, as shown in Fig. 1.7 [6].

Direct local ablative reshaping of an Au film was performed in [7] by irradiating it with tightly focused femtosecond laser pulses. The laser pulse locally melted a microscale area on the metal film, which detached from the underlying substrate and formed a cupola. The size of this cupola was controlled by the pulse power. Depending on its size, the cupola can resonantly scatter optical radiation, giving various pure colours from green to red [7].

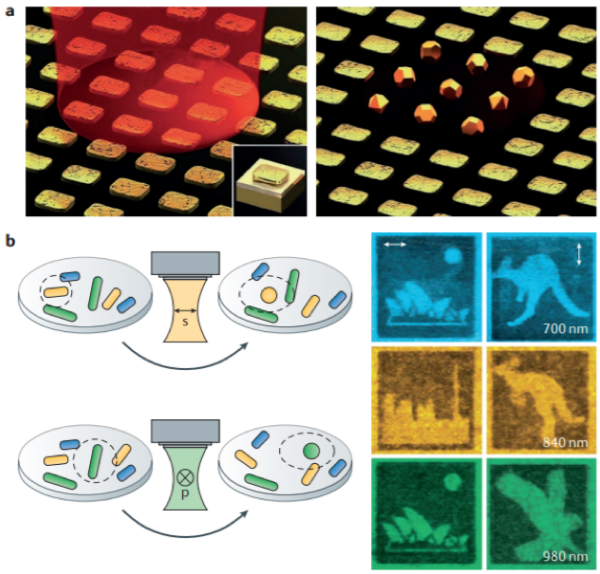

Figure 1.7: Patterning and storing information in structures, and morphology changes at the single-resonator level [6].

Lasers can be applied to create 3D photonic crystals with a resolution higher than 100 nm. Such resolution can be achieved due to two-photon polymerization, which allows concentrating absorption in a very small area of photopolymer. Fig. 1.8 shows the difference in the absorption areas initiated by ultraviolet and infrared light.

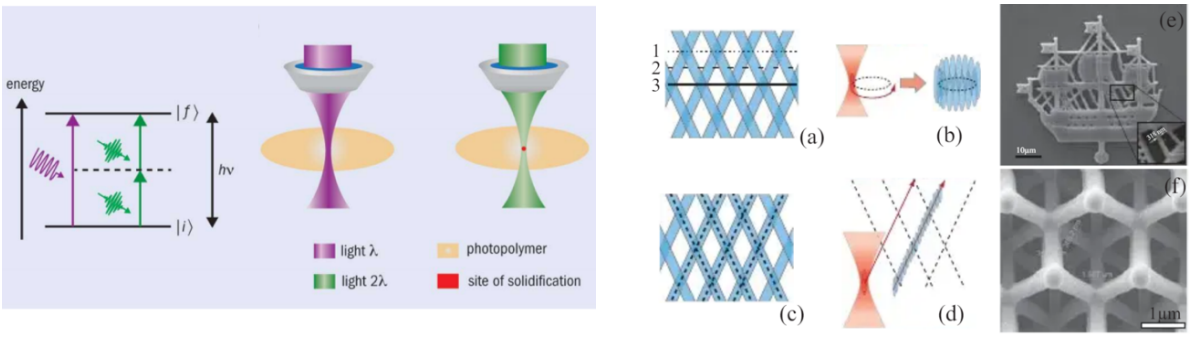

Figure 1.8: Absorption in a photopolymer initiated by ultraviolet and infrared light, and two methods for fabricating 3D structures by two-photon polymerization technology: raster scanning (a,b) and vector scanning (c,d); structures fabricated using raster (e) and vector (f) scanning approach. [8]

Periodicity in photon crystals can prevent light propagation in a certain direction, or create an omnidirectional complete photonic bandgap in a specific energy range. Fig. 1.8 shows structures created by the two-photon polymerization technique and two methods for their fabrication. To create such structures, femtosecond pulses centered at a wavelength of approximately 780 nm and with a repetition frequency of 80 MHz were used. As a source, a 50-fs TiF-100F laser emitter was used [8].

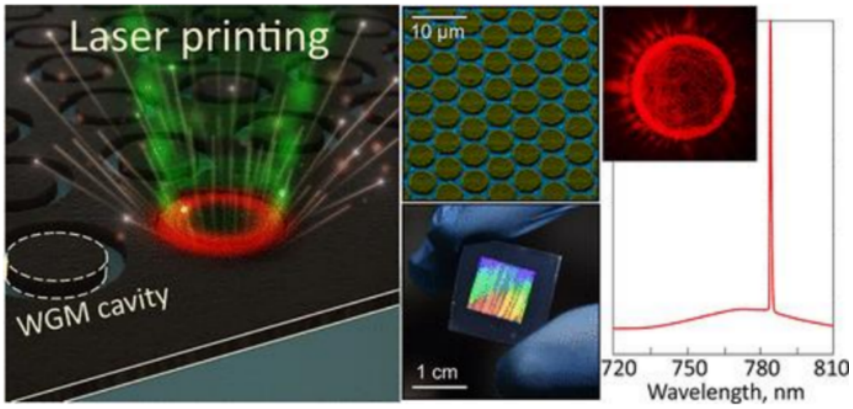

Figure 1.9: Single-mode lasing perovskite microdisks [9].

Furthermore, a laser can be used for the fabrication of another laser: for example, for the fabrication of protein-based 3D whispering gallery mode microlasers that are stimulus-responsive [9]. In this research, a laser with a 150 nm scanning step, 25-28 mW laser power and exposure time of 1000 μs at each point created 2.5 μm-thick laser microdisks.

Femtosecond lasers formed microlasers based on $MAPbBr_xI_y$ microdisks with a 760 nm thickness and diameters ranging from 2 to 9 μm on a perovskite film, shown in Fig. 1.9. The diameter of these microdisks was controlled by the intensity of the laser beam. This method allowed fabricating single-mode perovskite microlasers that operated at room temperature in the spectral range from 550 to 800 nm [8].

Laser printing of silicon nanoparticles is one of the most effective methods for their fabrication. Other fabrication techniques such as chemical methods, plasma synthesis, and laser ablation in air or liquids can produce silicon nanoparticles of various sizes, but they cannot provide control over their size or precise deposition. Lithographic methods are more complicated, and they do not allow fabricating spherical nanoparticles. One of the most effective ways to synthesize silicon nanoparticles of a certain size is laser printing. In ref. 11, this method was used with silicon-on-isolator (SOI) as a target, and spherical Si nanoparticles were transferred from a 50 nm crystalline Si layer onto a transparent glass receiver substrate. A femtosecond laser was used as a source of laser pulses at a wavelength of 800 nm and pulse power up to 3 mJ. The size of nanoparticles was controlled by the pulse power.

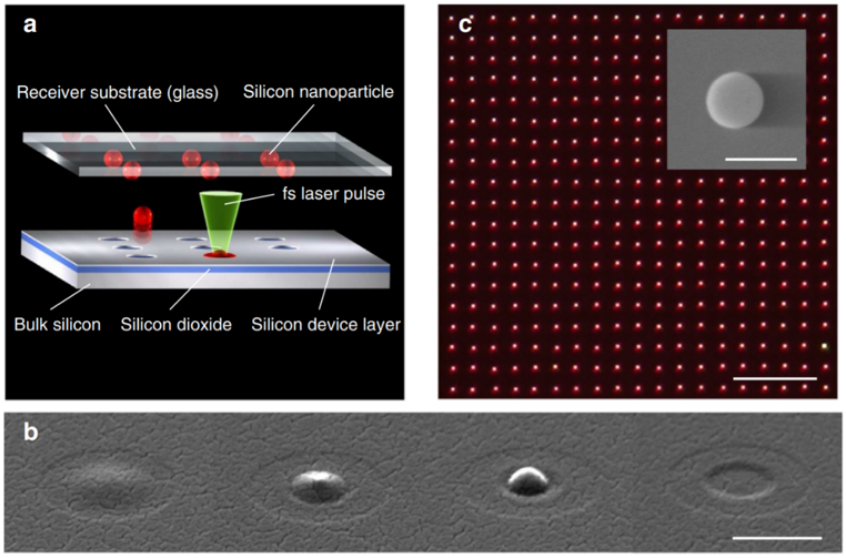

Figure 1.10: Laser-printing process of Si nanoparticles. (a) Schematic illustration of femtosecond laser printing of nanoparticles. (b) SEM images of the target before and after the nanoparticle-ejection process from the SOI substrate. From left to right, the laser pulse energy is gradually increasing. The scale bar is 400 nm. (c) Array of several hundreds of amorphous Si nanoparticles fabricated by this method. The scale bar is 20 μm. [11]

During the laser irradiation of the SOI wafer by a laser pulse, absorption in the top Si layer resulted in fast local heating and melting of that layer. If the energy of a pulse was high enough, the silicon layer melted completely, forming a droplet induced by the surface tension. That spherical droplet had an upward-directed momentum, which drove

it to the receiver substrate, where the liquid material solidified (Fig. 1.10) [9].

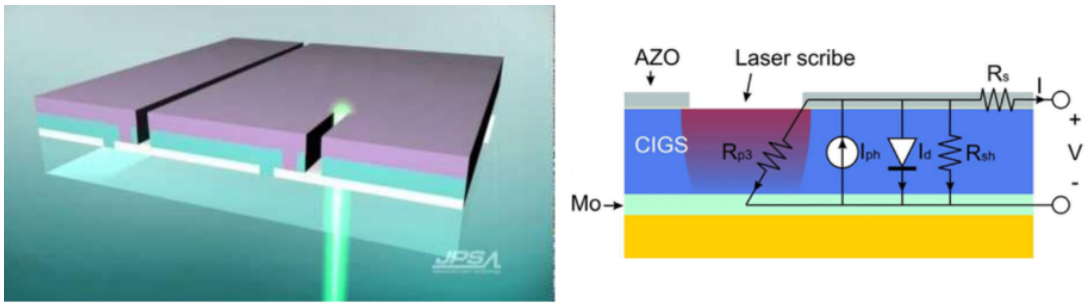

Figure 1.11: Laser scribing [12].

Another important laser application in optoelectronics is scribing (Fig. 1.11), which allows removing a single thin layer in a multilayer system without affecting the other layers. Laser scribing allows separating modules via cutting small pieces from a structure. Scribing is used in many semiconductor technologies characterized by relatively small substrates with required narrow separation lines. LED substrates are expensive, which makes their surface area highly valuable. Ultraviolet lasers provide narrow and clean cuts, and as a result, a higher throughput per substrate, and also higher yields due to the fact that they damage the surface less than the conventionalscribing methods.

Moreover, lasers can be applied for producing the so-called black silicon. This material is a surface modification of silicon with a low reflectivity and a high absorption of visible and infrared light. To obtain it, the silicon surface is irradiated with femtosecond laser pulses in the presence of sulfur hexafluoride gas or in a vacuum. As a result, micrometer-sized conestructure is created on the surface. This material has the absorption extending to the infrared range, below the band gap of silicon, including the wavelengths at which ordinary silicon is transparent.

Laser surface modification allows making super-hydrophobic coating, which is extremely difficult to wet. The contact angles of a water droplet on a super-hydrophobic material exceed 150° (Fig. 1.12). Such coating is extremely important for photovoltaics because of the improved absorption and additional protection from rain-related degradation.

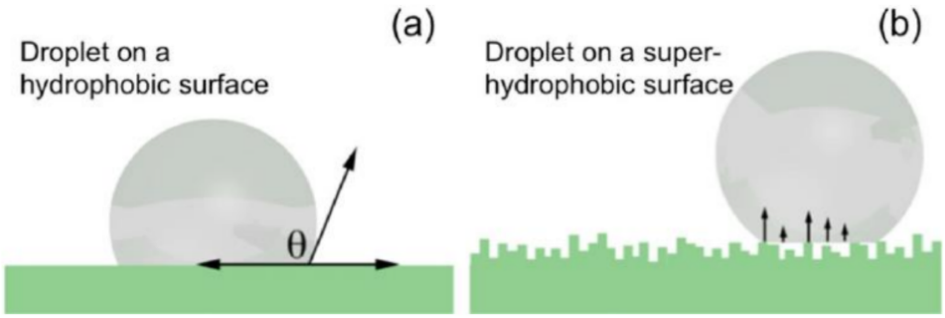

Figure 1.12: Hydrophobic (a) and super-hydrophobic (b) surface [13].

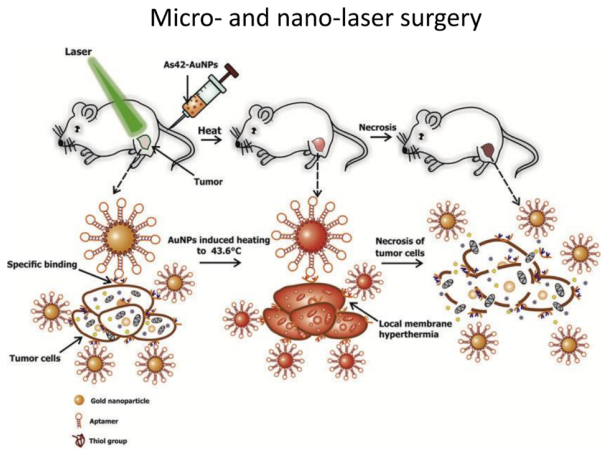

Figure 1.13: Micro- and nano-laser surgery for tumor cells removal [14].

Lasers also play an important role in medicine. They are applied for warts and tattoo removal due to heating and photochemical reactions. Femtosecond lasers are used in eye surgery, reshaping the front surface of the eye for better focusing. This can correct short-sightedness, long-sightedness and astigmatism. The UV light is absorbed in a very thin layer of the tissue, decomposing it into a vapour of small molecules, which fly away from the surface in a tiny plume. This happens so fast that nearly all the deposited heat energy is carried away in the plume, leaving too little energy behind to damage the adjacent tissue.

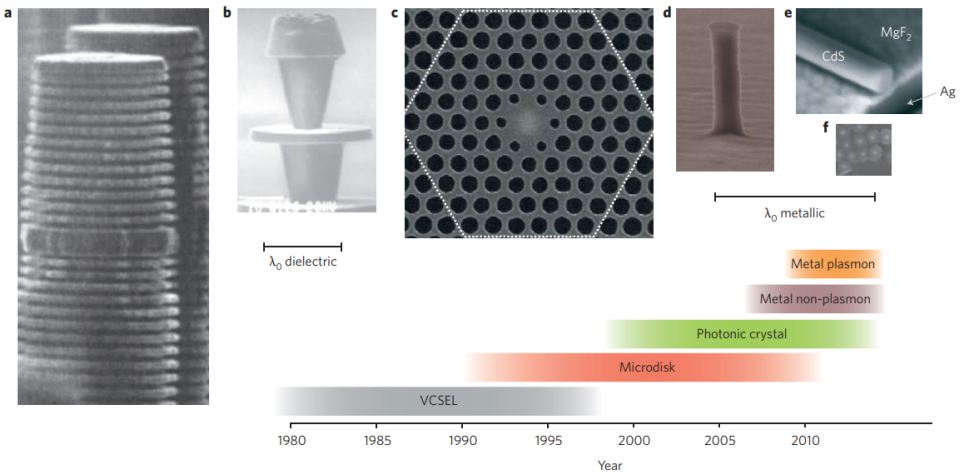

Figure 1.14: Progress in laser miniaturization and integration of photonic components. a) VCSEL b) Microdisk laser c) Photonic crystal laser d) Metallic non-plasmon mode laser e) Metallic propagating plasmon mode laser f) Localized plasmon mode laser. The free-space wavelength scale of metal cavity-based lasers (d-f) is half as lsrge as that of the dielectric lasers (a-c)[15].

One of the most promising laser applications in medicine is laser micro- and nanosurgery, which can provide removal of tumor cells (Fig. 1.13). First, nanoparticles are synthesized that absorb radiation at a specific wavelength, and they are covered with an additional organic material. These nanoparticles covered by an organic shell can bind only with a tumor cell. The laser irradiation used is rather weak so it does not damage the normal cells. However, its intensity is sufficient to heat the resonant nanoparticles and destroy the tumor cells that surround them.

The miniaturization and the integration of photonic components have improved such systems and opened up a wide variety of new application areas, somewhat similar to the advances in electronics. Applications of ever-smaller lasers include on-chip optical communications and data processing, which may allow data rates beyond those feasible in the realm of electronics. The progress in laser miniaturization over the past few decades is summarized in Fig. 1.14, with the images scaled to the lasing wavelength of the laser shown in each panel. It took 10-20 years since the initial proof-of-concept of lasing, which was often performed at low temperature, before the devices useful for applications were obtained.

Practical devices typically require continuous wave (CW) operation at room temperature, ideally with direct electrical pumping, a reasonably long lifetime and some particular characteristics that the existing types of lasers sometimes cannot offer. [15]

Questions

1. What does the abbreviation L.A.S.E.R. mean?
2. Which scientists contributed to LASER invention most significantly?
3. What are the main advantages of lasers as compared with the other light sources?
4. Describe basic principles of different applications of lasers in nanotechnology based on laser heating of the material.
5. Describe basic principles of different applications of lasers in nanotechnology based on photochemical processes induced by laser irradiation of materials.

References

1. https://en.wikipedia.org/wiki/Ruby_laser
2. https://global.canon/en/technology/s_labo/light/002/04.html
3. https://hothardware.com/news/intel-details-advanced-10nm-node
4. http://barrett-group.mcgill.ca/tutorials/nanotechnology/nano05.htm

5. Bäuerle D. Laser processing and chemistry. – Springer Science & Business Media, 2013.

6. Kristensen A. et al. Plasmonic colour generation //Nature Reviews Materials. – 2017. – V. 2. – №. 1. – P. 16088.

7. Wang X. et al. Single-step laser plasmonic coloration of metal films //ACS Applied Materials & Interfaces. – 2017. – V. 10. – №. 1. – P. 1422-1427.

8. Rybin M. et al. Band structure of photonic crystals fabricated by two-photon polymerization //Crystals. – 2015. – V. 5. – №. 1. – P. 61-73.

9. Sun Y. L. et al. Protein-based three-dimensional whispering-gallery-mode microlasers with stimulus-responsiveness //Scientific Reports. – 2015. – V. 5. – P. 12852.

10. Zhizhchenko A. et al. Single-Mode Lasing from Imprinted Halide-Perovskite Microdisks //ACS Nano. – 2019. – V. 13. – №. 4. – P. 4140-4147.

11. Zywietz U. et al. Laser printing of silicon nanoparticles with resonant optical electric and magnetic responses //Nature Communications. – 2014. – V. 5. – P. 3402.

12. Gečys P. et al. CIGS thin-film solar module processing: case of high-speed laser scribing //Scientific Reports. – 2017. – V. 7. – №. 1. – P. 1-9.

13. Schaeffer D. A. et al. Optically transparent and environmentally durable superhydrophobic coating based on functionalized SiO2 nanoparticles //Nanotechnology. – 2015. – V. 26. – №. 5. – P. 055602.

14. Kolovskaya O. S. et al. Aptamer-targeted plasmonic photothermal therapy of cancer //Molecular Therapy-Nucleic Acids. – 2017. – V. 9. – P. 12-21.

15. Hill M. T., Gather M. C. Advances in small lasers //Nature Photonics. – 2014. – V. 8. – №. 12. – P. 908.

Chapter 2

Properties of laser emission

2.1 Basic principles of lasers

To understand the main ideas behind a laser operation, the terms of induced absorption, spontaneous emission, and stimulated emission will be explained below. The terms mentioned will be described within the scope of a two-level system of an atom or a molecule with energies E_1 and E_2 ($E_1 < E_2$).

1. Induced absorption. In the case of a two-level system, a photon with sufficient energy enters to the system (according to Fermi's golden rule). The incident photon is absorbed by the atom in the ground state E_1, thereby leaving the atom in the excited state E_2.

2. Spontaneous emission. In this case, the atom emits a photon with energy $h\nu_0 = E_2 - E_1$ in any direction. This process,the so-called relaxation, can happen at any time, but the system should necessarily relax to the lowest state. This process is called spontaneous, because no external force is applied for it to start.

3. Stimulated emission. The mechanism of thisprocess is similar to that of spontaneous emission, but the atom is stimulated by an external photon. In this case, if the energy of the incident photon is equal to $h\nu_0 = E_2 - E_1$, then this photon induces the atom to decay to the ground state by emitting a photon that travels in the direction of the incident photon. Thus, we can get a coherent beam that is both amplified and unidirectional.

Turning to the concept of the probabilities of these processes, let us introduce N as the number of atoms or molecules per unit volume. The number N is referred to as the population of a level. Albert Einstein proposed the rates of these processes (i.e. the number of transitions per second) in 1916.

For the absorption rate, we can write

$$\frac{\partial N_1}{\partial t} = N_1 B_{12} \rho(\nu). \tag{2.1}$$

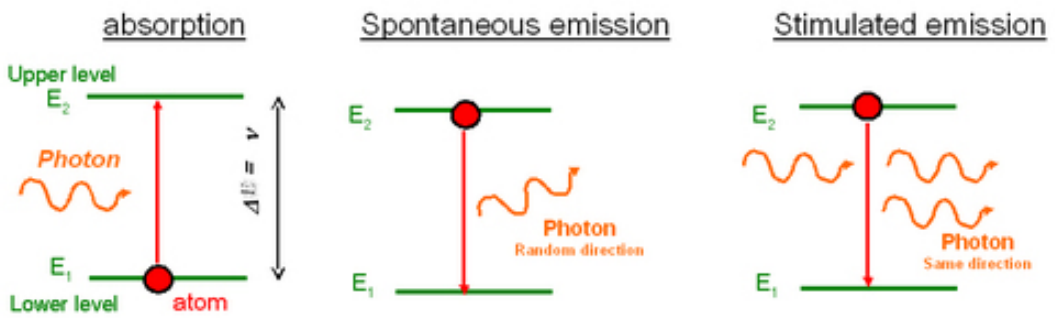

Figure 2.1: Mechanism of the interaction between an atom and a photon

For stimulated emission, we can write

$$\frac{\partial N_2}{\partial t} = N_2 B_{21} \rho(\nu). \tag{2.2}$$

Finally, the spontaneous emission rate is

$$\frac{\partial N_2}{\partial t} = N_2 A_{21}, \tag{2.3}$$

where N_1 is the population of the lower laser level 1, N_2 is the population of the upper laser level 2, $\rho(\nu)$ is the energy density of the incident radiation, A_{21} is the Einstein coefficient, or rate, of spontaneous emission, and B_{12} and B_{21} are the Einstein coefficients (or rates) for photon absorption and induced emission, respectively.

In thermal equilibrium, the populations of the two states 1 and 2 are determined by the Boltzmann distribution:

$$\frac{N_2}{N_1} = exp(\frac{-\Delta E}{kT}), \tag{2.4}$$

where ΔE is the energy difference between the two states, T is the temperature, and k is Boltzmann's constant. N_2 is always smaller than N_1 [1].

First, let us consider the Beer–Lambert–Bouguer law, which describes the exponential decrease of monochromatic light intensity as the light passes through an absorbing medium (Fig 2.2).

$$I = I_0 exp(-\alpha l), \tag{2.5}$$

where I is the intensity of the emergent beam, I_0 is the intensity of the incident beam, α is the absorption coefficient, and l is the length of the absorbing medium.

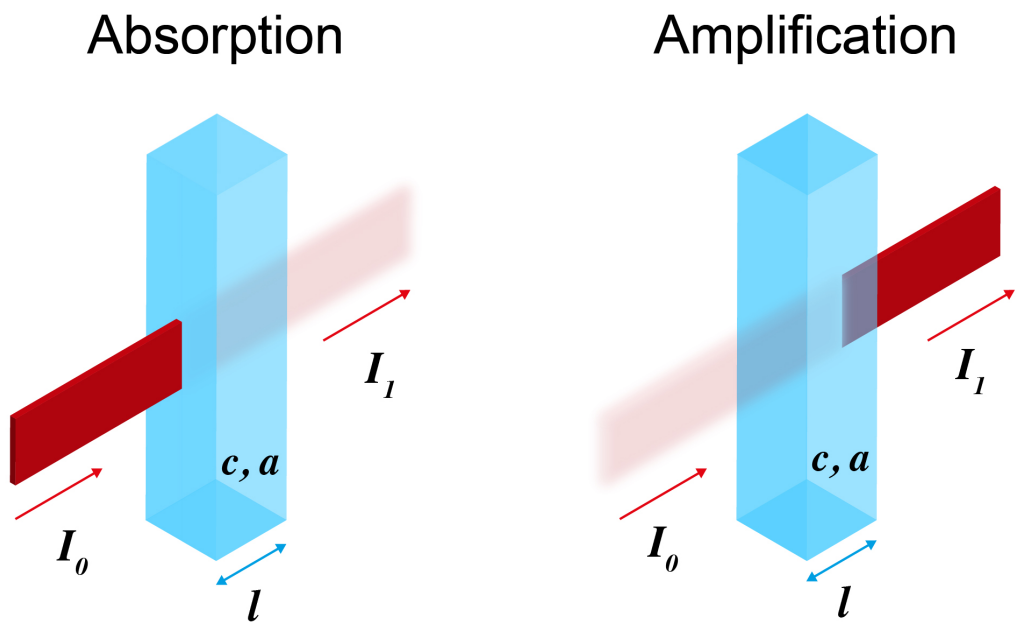

Figure 2.2: A schematic diagram of the absorption and amplification processes.

For a laser, strong stimulated emission is required, and as a consequence, a larger number of electrons in the upper state N_2 than in the lower state. This is called the population inversion ($N_2 > N_1$). The amplification is governed by the gain coefficient g (Fig. 2.2):

$$I = I_0 exp(+gl). \tag{2.6}$$

Let us consider the change in the intensity of a beam as it passes through a thin slice of material, as illustrated in Fig. 2.3:

$$\partial I = (N_2 B_{21} - N_1 B_{12}) \frac{I}{c} h\nu \partial z. \tag{2.7}$$

This is the difference between the stimulated emission and the absorption, i.e. the process opposite to amplification, and ∂z is the direction of propagation. We neglect the spontaneous emission.

Since B_{21}=B_{12}, we received:

$$\frac{\partial I}{\partial z} = (N_2 - N_1) B_{21} \frac{I}{c} h\nu. \tag{2.8}$$

Solving the differential equation, we obtain a law similar to the Beer law, but for amplification:

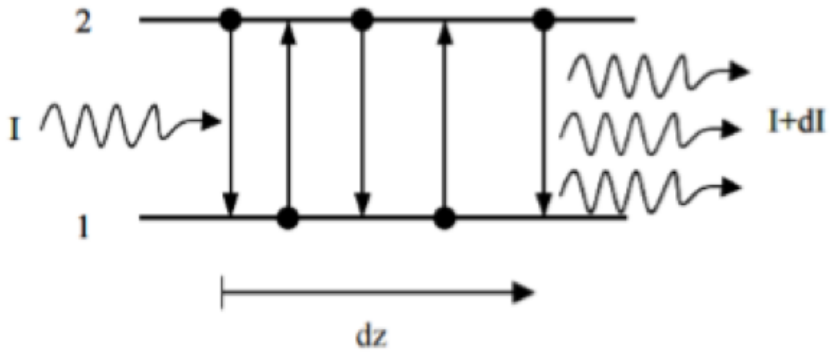

Figure 2.3: The change of the beam intensity as a beam passes through a slice of a material

$$I_z = I_0 exp(\gamma x), \tag{2.9}$$

where the "gain coefficient" γ is equal to g, which is given by

$$\gamma = (N_2 - N_1)B_{21}\frac{h\nu}{c} = (N_2 - N_1)\sigma = g, \tag{2.10}$$

where σ (cm^2) is the 'stimulated emission cross-section'. For the systems where we have separate atoms or separate ions that are generating light, all of them can be characterized by the stimulated emission cross-section. For $\gamma > 0$, the intensity of the light will increase as it passes through the material, i.e. there will be 'optical gain':

$$g(h\omega) = \frac{\pi e^2}{n_r c\varepsilon_0 m_0^2 \omega}|M|^2 \int_0^\infty \rho_r(f_c - f_\nu)\frac{\hbar/\pi\tau_{in}}{(E_g + E - \hbar\omega)^2 + (\hbar/(\tau_{in}))^2}\partial E. \tag{2.11}$$

where M is the transition probability, ρ_r is the density of states, τ_{in} is the carrier lifetime of intraband scattering (0.1 ps), f_c and f_ν are the Fermi distribution functions for electrons and holes, respectively, and f_c - f_ν is the population inversion [1].

Semiconductors can be classified into two types according to their energy bands in wavenumber space:

1. Direct band gap semiconductors (GaAs, InAs and some others);
2. Indirect band gap semiconductors (Si and Ge).

Fig. 2.4 shows a band energy diagram for direct band gap semiconductors, where the maximum of the valence band and the minimum of the conduction band have the same wave vector (k). In this case, the electrons-holes recombination is a direct process that involves only an emission of a photon.But in indirect band gap semiconductors (Fig. 2.4(b)), due to the different wave vectors of the maximum of the valence band and the minimum of the conduction band, the emission process requires an additional

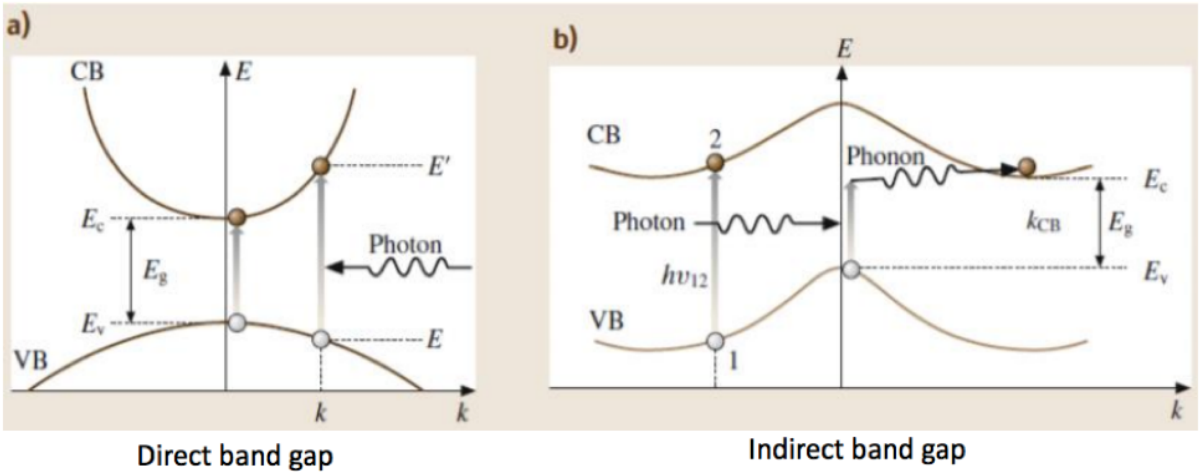

Figure 2.4: Schematic band diagrams for the emission processes in: (a) direct band gap semiconductors and (b) indirect band gap semiconductors

change of crystal momentum (i.e., involvement of a phonon). Photons cannot carry crystal momentum; therefore, the efficiency of emission in the indirect band gap semiconductors is much lower than that of direct band gap semiconductors [2].

The density of states (DOS) is the number of states at a particular energy level that electrons are allowed to occupy, i.e., the number of electron states per unit volume per unit energy. In semiconductors, the free motion of carriers can be limited to two, one, and zero spatial dimensions. When semiconductor statistics is applied to the systems of these dimensions, the density of states in quantum wells (2D), quantum wires (1D), and quantum dots (0D) is given by the following expressions:

3D (bulk):

$$g(E) = \frac{1}{2\pi^2}\left(\frac{2m^*}{\hbar^2}\right)^{3/2}\sqrt{E_g - E}. \tag{2.12}$$

2D (quantum well):

$$g(E) = \frac{m^*}{\pi\hbar^2}\sigma(E_g - E). \tag{2.13}$$

1D (quantum wire):

$$g(E) = \frac{m^*}{\pi\hbar}\sqrt{\frac{m^*}{2(E_g - E)}}. \tag{2.14}$$

0D (quantum dot):

$$g(E) = 2\delta(E_g - E), \tag{2.15}$$

where E_g is the band gap energy, m^* is the effective mass, $\hbar$ is the Plank constant and δ is the Dirac delta distribution function.

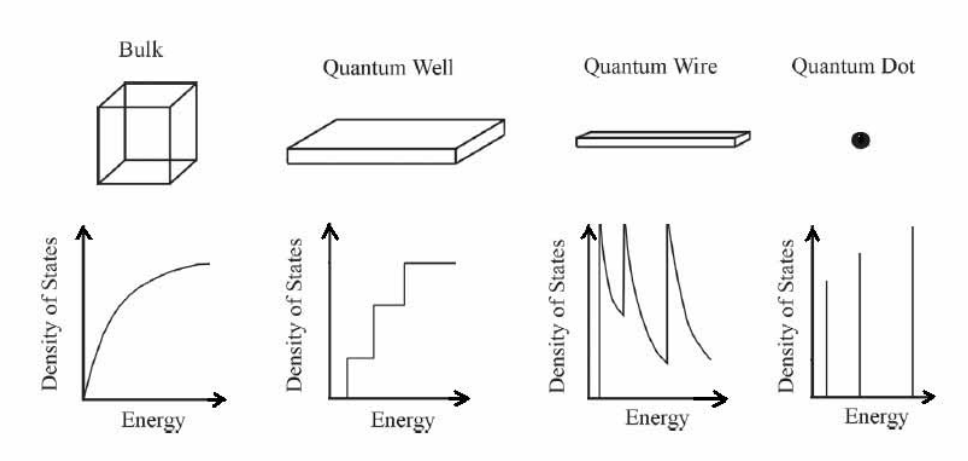

Figure 2.5: Density of states vs. energy for bulk material, quantum well, quantum wire and quantum dot

The variable stripe length (VSL) method is a very popular tool for measuring optical gain, demonstrated by Shaklee and Leheny in 1971 [3]. In the VSL method, the sample is pumped by an intense homogeneous laser beam, which is focused by a cylindrical lens to form a narrow stripe on the sample surface (Fig. 2.6). The length z of the stripe can be varied through a movable (variable) slit. When the stripe is short, the photoluminescence spectrum is broad. However, by increasing the length of the stripe, the emitted intensity increases super-linearly, and the spectrum becomes narrower. The same behaviour is observed if the pump energy is increased at a constant stripe length, as shown in Fig. 2.6. An amplified spontaneous emission (ASE) signal $I_{ASE}(z)$ is collected from the edge of the sample as a function of z. As a result of population inversion achieved at high pumping rates, spontaneously emitted light is amplified and an intense, and partially coherent ASE signal grows up exponentially increasing the excitation length z [4].

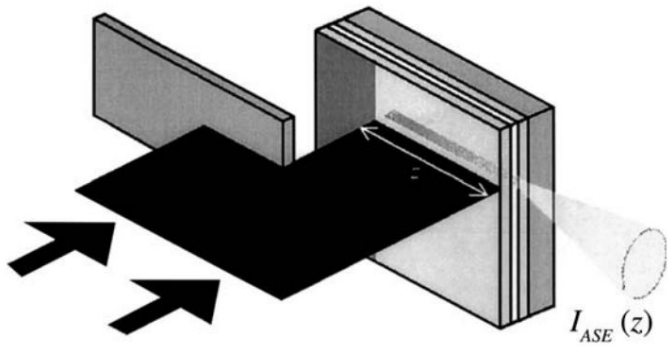

Figure 2.6: Sketch of the variable stripe length configuration. The amplified spontaneous luminescence intensity I_{ASE}(z) is collected from the edge of the sample as a function of the excitation length z. The laser beam is focused on a thin stripe by a cylindrical lens [4].

An important advantage of this widely used experimental method is that no special sample preparation is needed, and that both transparent and opaque samples are equally suited for gain measurements. In addition, the basic principle of the technique is extremely simple: a one-dimensional amplifier model.

To analyze the measured data, let us consider an optical amplifier in the form of an illuminated stripe, where the stripe width is very small compared to its length. This one-dimensional optical amplifier has a cylindrical shape with the length l and the cross-sectional area s. We accept I(z) as the ASE intensity at coordinate z for the beam propagating in the positive z-direction.

The elemental variation, ∂I, along the z-coordinate, does not only have to account for the stimulated emission but also for the spontaneous-emission contribution arising from the element ∂z. The solid angle seen from zero position is Ω, and the solid angle of the differential element ∂z is Ω(z) (Fig. 2.7). In the low saturation regime, the intensity from the differential element ∂z, which is emitted from the facet of the amplifier, consists of stimulated emission and spontaneous emission, which is radiated uniformly over the whole solid angle, and this can be written as:

$$\frac{\partial I}{\partial z} = (\Gamma g_m - \alpha)I + (S_{sp}N^*h\nu)(\frac{\Omega(z)}{4\pi}), \tag{2.16}$$

where Γ is the confinement factor for the waveguide structure, g_m is the material gain, α is the propagation loss coefficient, S_{sp} is the spontaneous emission rate, I is the intensity, N^* is the excited state population density and $h\nu$ is the energy of the emitted photon.

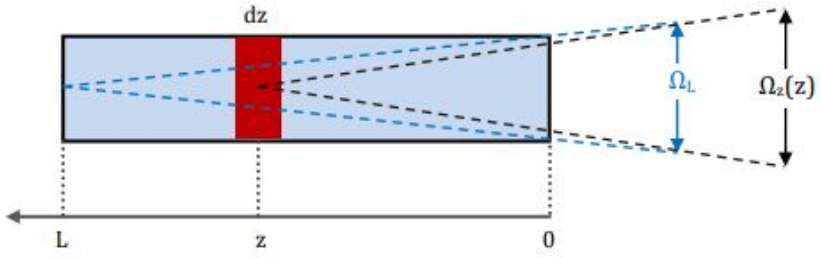

Figure 2.7: ASE along the illuminated stripe [3].

The gain and the pump intensity are assumed to be constant over the entire pumping length, and the equation above can be easily integrated using the boundary condition $I_{ASE}(0) = 0$. Applying the boundary condition, the ASE emission can be written as:

$$I_{ASE}(z) = \frac{J_{sp}(\Omega)}{g}(e^{gz} - 1), \tag{2.17}$$

where $J_{sp}(\Omega) = \frac{A_{sp}N^*h\nu\Omega}{4\pi}$ is the spontaneous emission intensity within the solid angle Ω; g is the net modal gain of the material, defined as $g = \Gamma g_m - \alpha$. For simplicity, we

will consider Γ=1 and α=0. The net modal gain of the material can be calculated by fitting the experimental data to the Eq.2.17. Tab. 2.1 shows optical gain values for several semiconductor materials measured with VSL.

Semiconductor material		Optical gain for 10^7 W/cm^{2}and 2 °K (cm^{-1})	Wavelength of the peak gain (nm)
III-V	GaAs	2000	820
	GaP : N	10000	540
	GaP : Bi	175	555.4
	GaN	1000	359
II-VI	CdS	200	490.5
	CdSe	1000	684
I-VII	CuCl	6400	392
III-VI	GaSe	10000	600

Table 2.1: Optical gain measurements for various semiconductor materials [5].

Thus, in order to create a laser, we need three main things:

1. Pump source. It will deliver external energy to the system. It will be converted into light.

2. Active medium. It is necessary for achieving the amplification of light and for the coherence of radiation.

3. Resonator. It will provide positive feedback and directivity of the generated radiation.

Gain and cavity

Optical gain is not sufficient to obtain laser operation, i.e. oscillation of light in a resonator. For lasing, we need to provide a good cavity. A cavity is required because it provides positive feedback, enabling photons to pass multiple times in the active medium and amplify the signal repeatedly (Fig. 2.8). For oscillation, we need:

1. Gain $\geqslant$ losses, i.e. $\gamma \geqslant \alpha$ (where the loss coefficient is $\alpha > 0$). When the losses and gain are equal, we have reached the lasing threshold. If the gain is lower than the losses, it leads to a decrease in energy (absorption). Losses can result from roughness, impurities, and other defects.

2. Positive feedback. For $\gamma > 0$, the condition $N_2 > N_1$ is required. However, for any thermal population, the distribution is $N_2 < N_1$ Therefore, we need to excite, or 'pump'

the material, known as the 'gain medium', to get $N_2 > N_1$ (usually, by illuminating it with another light source or by passing electric current through the material). The condition of N=$N_2 - N_1 > 0$ is known as 'population inversion'.

Now the rate equation takes the form:

$$N_2 = -N_2 B_{21}\rho - A_{12}N_2 + N_1 B_{12}\rho + R, \tag{2.18}$$

where R is the pump rate, i.e. the rate of excitation to level 2.

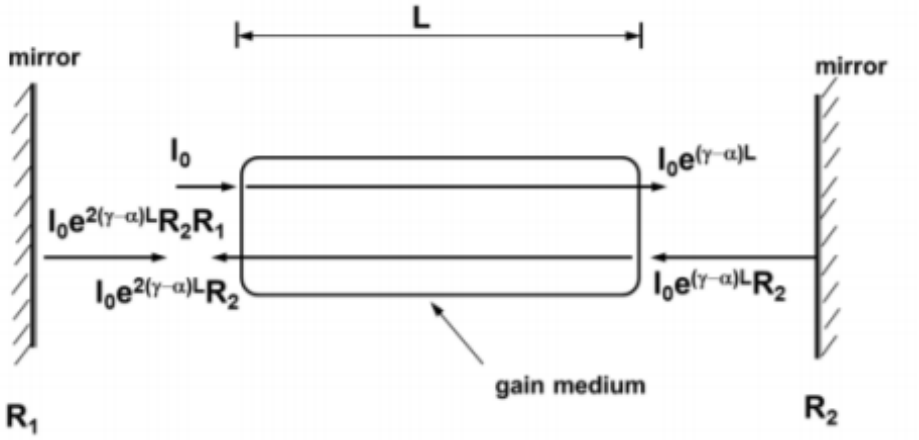

Figure 2.8: Gain and loss during a round trip of light through the cavity

Normally, photons are randomly emitted from the active medium, and only a small part of these photons emitted along the axis of the resonator, start to propagate in the above direction multiple times (Figure. 2.8). After passing through the gain medium for the first time, this part experiences the net gain (i.e. the gain minus the loss), and the intensity is

$$I = I_0 e^{(\gamma-\alpha)L} \tag{2.19}$$

and after the subsequent reflection from the right-hand mirror, the intensity becomes:

$$I = I_0 e^{[(\gamma-\alpha)L]R_2}, \tag{2.20}$$

where $R_{1,2}$ are the reflection coefficients of cavity mirrors, L is the length of the active medium.

Then this light passes back through the gain medium, and at this point, the intensity is

$$I = I_0 e^{[2(\gamma-\alpha)L]R_2}. \tag{2.21}$$

Then the light is reflected by the left-hand mirror, so that when it returns to its starting position, the intensity becomes:

$$I = I_0 e^{[2(\gamma-\alpha)L]R_1R_2}. \tag{2.22}$$

For steady-state operation, we require that the intensity does not change after one round-trip, i.e.

$$I_0 = I_0 e^{[2(\gamma_{th}-\alpha)L]R_1R_2}. \tag{2.23}$$

where γ_{th} is the "threshold gain coefficient", and this is the gain required only to compensate for the total losses (such as absorption and scattering in the gain medium, and transmission through the mirrors). Re-arranging this expression, we obtain:

$$\gamma_{th} = \alpha - 1/(2L) \cdot ln(R_1R_2) \tag{2.24}$$

Resonators

The most widely used laser resonators have either plane or spherical mirrors, separated by the distance L. Typically, L may range from a few centimetres to a few dozen centimetres, while the mirror dimensions range from a fraction of a centimetre to a few centimetres. The resonator length is usually much greater than the laser wavelength, as the latter usually ranges from a fraction of a micrometre to a few dozen micrometres. A laser cavity with the length comparable to the wavelength would have a gain too low for laser oscillation. Laser resonators are usually open, because this drastically reduces the number of modes that can oscillate with low losses.

Among the various possible resonators, we particularly mention the following types, illustrated in Fig. 2.9 ($R_{1,2}$ are the curvatures radii of the mirror):

1. Plane-parallel (Fabry-Perot) resonator $R_1 = R_2 = \infty$. It consists of two plane mirrors set parallel to each other.

2. Spherical cavity resonator $R_1 = R_2 = \mathrm{L}/2$. This resonator consists of two spherical mirrors having the same radius R and separated by the distance L, so that the mirrors centres of curvature C_1 and C_2 coincide (i.e. L = 2R).

3. Confocal cavity resonator $R_1 = R_2 = \mathrm{L}$. It consists of two spherical mirrors of the same radius of curvature R separated by a distance L so that the mirror foci are coincident. It then follows that the center of curvature C of one mirror lies on the surface of the second mirror.

4. Concave-convex resonator $R_1 > L$, $R_2 > L$. This design produces no intracavity focusing of the beam, and thus, it is useful in high-power lasers, in which the intensity of the intracavity light might be damaging to the intracavity medium, if brought to a focus.

For any resonant system, and in particular, for a resonant optical cavity, the cavity Q factor (normally referred to as the cavity Q) is Q=2·(energy stored)/(energy lost in one

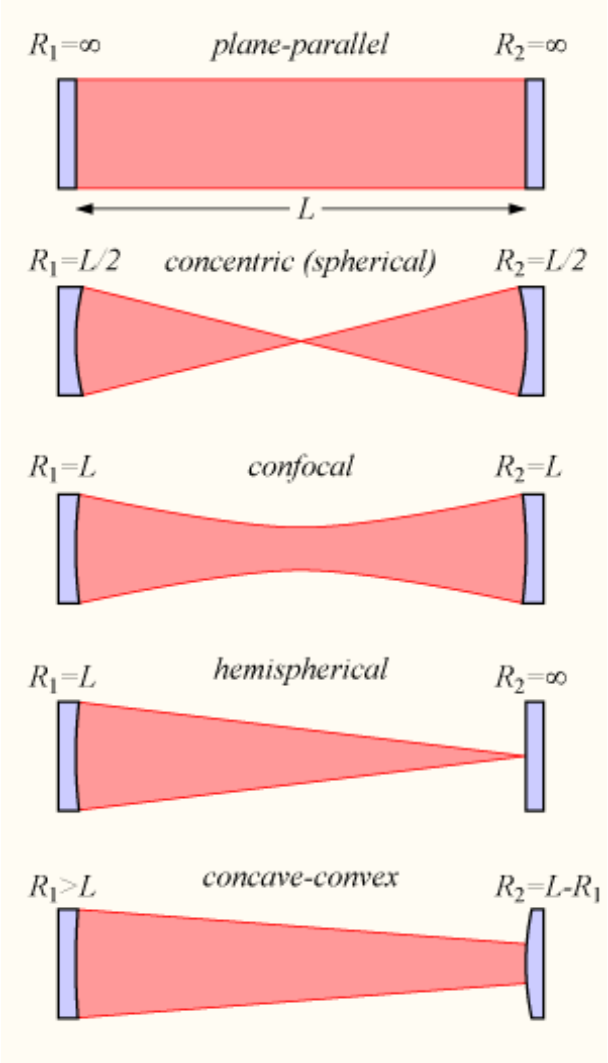

Figure 2.9: Types of two-mirror optical cavities, with mirrors of various curvatures, and the radiation patterns inside each cavity.

cycle of oscillation). The quality factor, or 'Q', of an inductor or a tuned circuit is often used to indicate its performance in a resonator circuit. It also provides an indication of the resonator's bandwidth with respect to its center frequency.

The concept of Q, Quality Factor, was first proposed by K. S. Johnson, an engineer from the Engineering Department of the Western Electric Company in the US. He was evaluating the performance and quality of various coils, and developed the concept of Q. Interestingly, he chose the letter Q because all other letters of the alphabet were already engaged, rather than because of the term Quality Factor itself, although with hindsight, the choice of the letter Q for a quality factor could not have been any better.

The Q factor is a dimensionless parameter that indicates energy losses within any resonant element, from a mechanical pendulum, an element in a mechanical structure or

in an electronic circuit:

$$Q = \frac{\lambda}{\Delta\lambda}, \tag{2.25}$$

where λ is the resonant wavelength, and $\Delta\lambda$ is the resonance width, or full width at half maximum.

The Q factor is limited due to the losses in the material (the lower the losses, the higher Q), which can be written as:

$$1/Q = 1/Q_{nr} + 1/Q_r \tag{2.26}$$

where Q is the total quality factor of the resonator, Q_{nr} describes the non-radiative contributions to the quality factor, and Q_r describes the radiative contributions to the quality factor (the first channel is leakage, the second channel is roughness).

Basic equations for lasing

Considering the population of electron-hole pairs that are generated due to the e-h pairs intraband transition, the kinetics of this process is described by the following equation:

$$\frac{\partial n}{\partial t} = \eta_p \frac{P}{\hbar\omega_p V_\alpha} - R_{nr}(n) - R_{sp}(n) - R_{st}(n)s, \tag{2.27}$$

where n is the carrier density, s is the photon density, η_p is the absorption efficiency, P is the power of the incident light, $\hbar$ is the Plank constant, ω_p is the frequency of the incident light, V_a is the volume where the light is absorbed, and R_{nr}, R_{sp} and R_{st} are the nonradiative, spontaneous emission and stimulated emission rates, respectively.

The photon density in the cavity mode is described by the kinetic equation for lasing photons:

$$\frac{\partial s}{\partial t} = -\frac{s}{\tau_p} + \Gamma\beta_{sp}R_{sp}(n) + \Gamma R_{st}(n)s, \tag{2.28}$$

where τ_p is the lifetime of photons in lasing mode, Γ is the energy confinement factor, and β_{sp} is the spontaneous emission coupling factor.

In the case when speed is negative, the absorption lifetime of photons in lasing mode is:

$$\tau_p = Q/\omega. \tag{2.29}$$

The rate of spontaneous emission can be written as:

$$R_{sp} = n/\tau_{sp}, \tag{2.30}$$

while the stimulated emission rate is:

$$R_{st} = \nu_g g(n). \tag{2.31}$$

The gain g(n) can be written as:

$$g(n) = g_0 ln(\frac{n + N_s}{N_{tr} + N_s}), \tag{2.32}$$

where g_0, N_s and N_{tr} are material parameters associated with the intrinsic gain of the active medium.

2.2 Basic properties of laser emission

There are several properties that characterize laser emission: high monochromaticity, coherence, directionality, brightness, and duration. In the following sections, we will consider these properties in more detail.

Monochromaticity

Light is called monochromatic in case all the photons emitted by a laser have the same energy and the same wavelength (i.e. the light has a single spectral colour). Unfortunately, laser light cannot be truly monochromatic, because this would have required a wave train of infinite duration. Any spectral emission line has a finite width because of the Doppler effect caused by the moving atoms or molecules that emit photons. Compared to ordinary sources of light, the spectral width (the linewidth) of a laser is extremely small.

The following factors are responsible for monochromaticity of a laser beam:

1. Only an electromagnetic wave with the frequency $\nu_0 = E_2$-E_1 can be amplified. ν_0 has a certain spectral width, which is called linewidth, defined by homogeneous and inhomogeneous broadening factors.

2. Lasing implies that the laser cavity forms a resonant system, and laser oscillation is sustained only at the resonant frequencies of the cavity. This leads to a further narrowing of the laser linewidth.

The degree of monochromaticity can be quantitatively described in terms of linewidth. The narrower the linewidth, the higher the monochromaticity is. However, this depends on the type of laser, and special techniques can be used to improve monochromaticity. The typical linewidth of a commercial He-Ne laser is about 1500 MHz (full width at half-maximum, FWHM). In terms of wavelength, it means that at a wavelength of 632.8 nm, the linewidth is approximately 0.01 nm.

Coherence

Apart from spontaneous emission, an excited atom can be induced to emit a photon by another photon of the same frequency, i.e. a passing photon can stimulate a transition from a higher level to a lower level, resulting in the emission of two photons, which means a gain. The two emitted photons are in phase, which means that the maxima and minima of the wave associated with one photon occur at the same time as for the wave associated with the other photon.

An avalanche of similar photons is created, and these photons have the frequency, the phase, the polarization, and the direction of propagation equal to those of the incident photons, which results in generation of a coherent laser beam.

Coherence is a property of waves that indicates their ability of stationary interference. Two coherent waves can be combined to produce an unmoving distribution of constructive and destructive interference (a visible interference pattern) depending on the value of their phase difference, which should be constant. Using a Michelson interferometer, one can estimate the coherence length by measuring the maximum path difference between the two beams, which still show the interference pattern (Fig. 2.10).

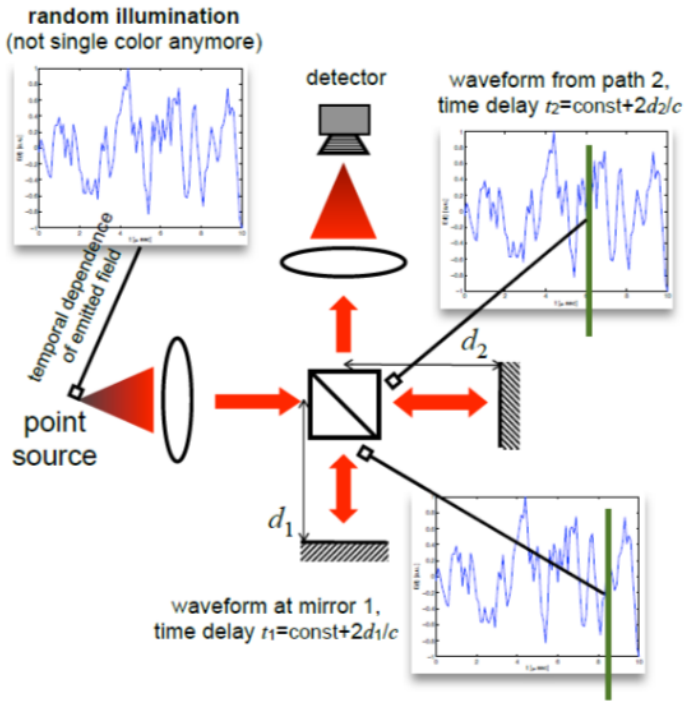

Figure 2.10: Michelson interferometer

The correlation between the wave and the same wave delayed by some time at the same location at different times or in different locations along the path of a beam at the same moment (that are effectively the same thing), is called temporal coherence. Let us consider a single point on the wavefront. The wave will have a phase difference between

the points in time $t = 0$ and $t = dt$. If this phase difference remains the same for any value of dt, then we say that the electromagnetic wave has perfect temporal coherence. But if this is true only for a specific value of dt, then the electromagnetic wave has partial temporal coherence.

If a wave is combined with a delayed copy of itself, the duration of the delay over which it produces visible interference is known as the coherence time of the wave, τ_{coh}. Based on this time, the corresponding coherence length L_c can be estimated as:

$$L_c = c\tau_{coh} = c/(\pi\Delta\omega). \tag{2.33}$$

A line-broadening mechanism is referred to as homogeneous when it broadens the line of each atom in the same way. In this case, the line shape of the single-atom cross-section and that of the overall absorption cross-section would be identical. There is some internal mechanism of broadening in each atom. Each atom experiences the same broadening mechanism because broadening is caused by some collisions. All atoms emit the same spectrum with the same centre frequency ν_0. Consequently, the resulting spectrum has a Lorentzian shape. This line shape is observed in Nd^3+, YAG, CO_2 and other lasers.

A line-broadening mechanism is said to be inhomogeneous when it distributes the atomic resonance frequencies over some spectral range. Such a mechanism thus broadens the overall line of the system without broadening the lines of individual atoms. Different atoms emit at slightly different central frequencies, due to random processes shifting the peak frequency. Each atom is an oscillator, and this results in a Lorentzian shape for each atom. An example of such a laser is He-Ne laser.

Let us take two points on a wavefront, at a time point equal to zero. There will be a certain phase difference between these two points and if it remains the same even after a lapse of a period of time, then the electromagnetic wave has perfect coherence between the two points. In case the phase difference remains the same for any two points anywhere on the wavefront, then we say that the electromagnetic wave has perfect spatial coherence, whereas if this is true only for a specific area, then the electromagnetic wave is said to have only partial spatial coherence. Spatial coherence is related to directionality and uniphase wavefronts. Some randomness in the phase in the space appears, because of random emission of the light source within one source. Spatial coherence describes the ability for two points in space, x_1 and x_2, in the extent of a wave to interfere, when averaged over time. More precisely, the spatial coherence is the cross-correlation between two points in a wave for all times.

Spatial coherence is high for spherical waves and plane waves and is related to the size of the light source. A point source emits spatially coherent light, while the light from a finite source has a lower coherence. Spatial coherence can be increased with a spatial filter which is a very small pinhole preceded by a condenser lens. The spatial coherence of light will increase as it travels away from the source and becomes more like a sphere or a plane wave. The light from distant stars, though far from being monochromatic, has extremely high spatial coherence.

Coherence length is defined as the length over which energy in two separate waves remains constant. As for the laser, it is the greatest distance between thw two arms of an interferometric system for which sufficient interferometric effects can be observed. For a random source, the coherence length can be estimated as follows:

$$r_c \sim \frac{\lambda z}{a}, \tag{2.34}$$

where z is the distance to the source and a is the size of the source. For a laser, the coherence length will be approximately equal to the beam radius.

Directivity

Another advantage besides coherence is directivity. A laser beam is highly directional, which implies that a laser light has very small divergence. This is a direct consequence of the fact that a laser beam comes from the resonant cavity, and only the waves propagating along the optical axis can be sustained in the cavity. Directionality is described by the light beam divergence angle.

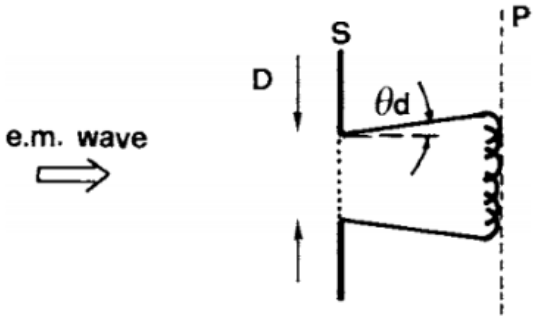

Figure 2.11: Divergence of a plane EM wave due to diffraction. A monochromatic beam of uniform intensity and plane wave-front is assumed to be incident on a screen S containing an aperture D. According to Huyghens' principle the wave-front at some plane P behind the screen can be obtained from the superposition of the elementary waves emitted by each point of the aperture. We thus see that, on account of the finite size D of the aperture, the beam has a finite divergence θ_d.

For perfect spatial coherent light, a beam of aperture with a diameter D will have an unavoidable divergence because of diffraction. From diffraction theory, the divergence angle θ is:

$$\theta = \frac{\beta\lambda}{D}, \tag{2.35}$$

where λ and D are the wavelength and the diameter of the beam, respectively (see Fig. 2.11). The factor β is a numerical coefficient of the order unity whose value depends

on the shape of the amplitude distribution and on the way both the divergence and the beam diameter are defined.

If the beam has a partial spatial coherence, its divergence is bigger than the diffraction limited divergence. In this case the divergence becomes:

$$\theta_{pc} = \frac{\lambda}{S^{1/2}}. \tag{2.36}$$

where S is the coherence area.

Duration

Laser pulse duration is the time during which the laser output pulse power remains continuously above half its maximum value. The optical power appears in pulses of some duration at some repetition rate. The duration of optical pulses (also called pulse width or pulse length) can vary in a huge range:

1. "Infinite" – continuous-wave lasers ($t = \infty$). Continuous-wave lasers produce a continuous, uninterrupted beam of light, ideally with a very stable output power.
2. Mechanical shatter ($t > 1$ μs)
3. Q-switching: Pockels cell ($t > 0.1$ ns)
4. Mode-locking ($t > 1$ fs)

The Fig.2.12 demonstrates the reduction of the pulse duration over years.

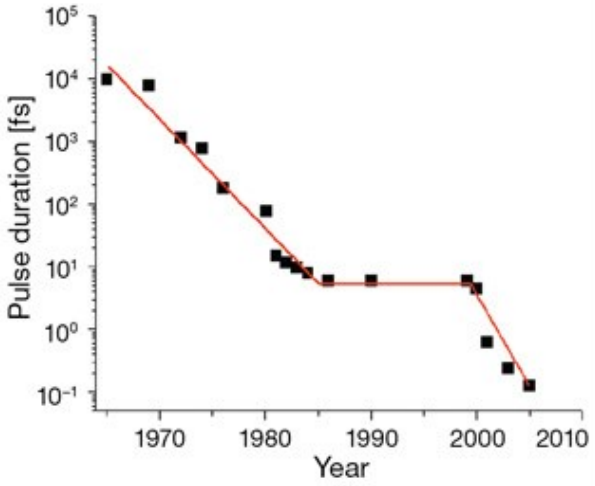

Figure 2.12: Minimum duration of achievable laser-like pulses over time

Basic characteristics of pulsed laser

Pulsed lasers are versatile tools for scientists and engineers that have played an important role in the development of modern optical physics. The first laser, invented by T. H.

Maiman, was a pulsed laser. In that laser, a ruby crystal (chromium-doped sapphire) served as the gain medium, which was excited by the light from a pulsed flashlamp that surrounded the crystal. Two parallel faces of the crystal were coated with silver, which served to trap photons emitted along the optic axis so that they would pass through the crystal many times before escaping. The laser operated at room temperature and produced pulses of light with a wavelength of 694 nm (near-infrared).

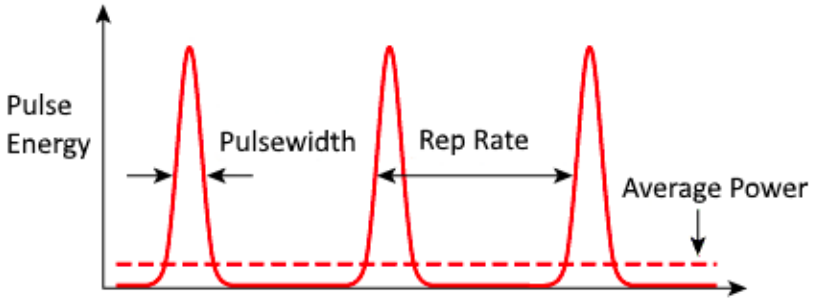

Figure 2.13: Characteristics of pulsed laser. Pulsed lasers emit bursts of light, spaced in time. There is no emission between the pulses.

There are several important parameters of a pulse laser:
1) Pulse duration (s) - τ
2) Repetition rate (Hz) – RR (reversed distance between pulses)
3) Energy per pulse (J) – E (the number of photons in the pulse)
4) Average power (W) – P_{av} (the amount of energy during the period of time). This can be calculated as:

$$P_{av} = E \cdot RR. \tag{2.37}$$

5) Peak power (W) - P_{peak} (power in each laser pulse). This can be calculated as:

$$P_{peak} = E/\tau. \tag{2.38}$$

6) Beam size (cm) – D
7) Fluence (J/m^2) – F (density of power). This can be calculated as:

$$F = E/S = \frac{4E}{(\pi D^2)}. \tag{2.39}$$

8) Intensity (W/cm2) – I, which can be calculated as:

$$I = F/\tau. \tag{2.40}$$

9) Average intensity (W/cm2), which can be calculated as:

$$I = W \cdot RR. \tag{2.41}$$

Some basic parameters of a laser pulse are illustrated in Fig.2.13.

Questions

1. Which three optical processes do govern population of energy levels in an active medium in laser?
2. What are the main types of spectral broadening?
3. What is the minimum number of energy levels needed to create a laser?
4. Name the basic properties of laser radiation.

References

1. Svelto O., Hanna D. C. Principles of lasers. – New York : Plenum press, 1998. – V. 4.
2. Kasap S., Capper P. (ed.). Springer handbook of electronic and photonic materials. – Springer, 2017.
3. Shaklee K. L., Leheny R. F. Direct determination of optical gain in semiconductor crystals //Applied Physics Letters. – 1971. – V. 18. – №. 11. – P. 475-477.
4. Dal Negro L. et al. Applicability conditions and experimental analysis of the variable stripe length method for gain measurements //Optics communications. – 2004. – V. 229. – №. 1-6. – P. 337-348.
5. Hill, M.T. and Gather, M.C., 2014. Advances in small lasers. Nature Photonics, 8(12), p.908.

Chapter 3

Short and Ultrashort Laser Pulses

3.1 Introduction

Herein we will discuss in some detail the methods by which lasers can be designed to produce short and ultrashort light pulses. First, however, we will give a brief and simple review of lasers in general, as well as of stationary and quasi-stationary laser behaviour.

3.2 Relaxation oscillations

We first first consider the case of a step-function pump rate. We assume that $R_p = 0$ for $t < 0$ and $R_p(t) = R_p$ (independent of time) for $t > 0$, R_p is pump repetition rate. We also assume the laser to be oscillating in a single mode so that a simple rate-equation treatment can be properly applied. The rate equations are nonlinear in the variables $N(t)$ and $\phi(t)$ (photon number) since they involve products of the form ϕN. Consequently, analytical solutions for this case or for other cases to be considered, do not appear to be possible, and we often have to resort to numerical computation.

As a representative example, Fig. 3.1 shows one of the first computed plots of $N(t)$ and $\phi(t)$ carried out for a three-level laser. In this case the initial condition for the population inversion is $N(0) = -N_t$, where N_t is the total population, because, at the time point $t = 0$, the entire population is in the lower laser level. The initial condition for the total number of cavity photons is then $\phi(0) = \phi_i$, where ϕ_i can be assumed to be some small integer (e.g. $\phi_i = 1$) which would be only needed to let the laser action start. Such regular oscillation for the output power is usually referred to as a damped relaxation oscillation. The time behaviour of the population inversion then undergoes a similar oscillatory behaviour, the oscillation of $N(t)$ leading that of $\phi(t)$ by about half the oscillation period since there first has to be a population rise of $N(t)$ to then produce a corresponding rise of the photon number, $\phi(t)$. It also has to be noted that a similar

behaviour to that in Fig. 3.1 is also expected for a four-level laser, one of the main differences being that, in the latter case, the initial condition is $N(0) = 0$.

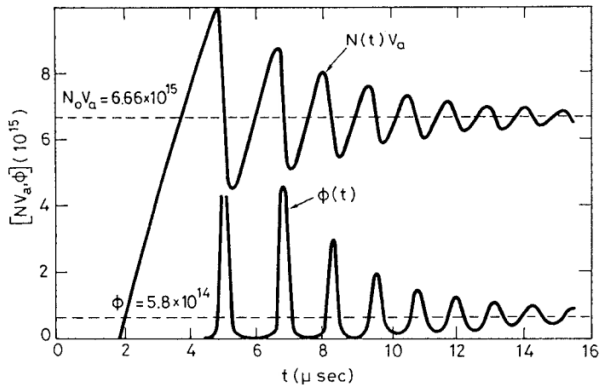

Figure 3.1: Example of the temporal behavior of total inversion, $V_a N(t)$, and photon number, $\phi(t)$, for a three-level laser

For small oscillations about the steady-state values (for $t > 15\mu s$ in Fig. 3.1), the dynamical behavior can be described analytically. We can write:

$$N(t) = N_0 + \delta N(t), \tag{3.1}$$

$$\phi(t) = \phi_0 + \delta\phi(t), \tag{3.2}$$

and assume $\delta N \ll N_0$ and $\delta\phi \ll \phi_0$, we can neglect the product $\delta N \delta\phi$ in the expression $N\phi$ appearing in the rate equations, and these equations become linear in the variables δN and $\delta\phi$.

Reducing to the case of a four-level laser, we can write

$$\frac{dN}{dt} = R_p - B\phi N - \frac{N}{\tau}, \tag{3.3}$$

$$\frac{d\phi}{dt} = \left(BV_a N - \frac{1}{\tau_c}\right)\phi \tag{3.4}$$

where R_p is the pumping rate, B is the coefficient referred to as the stimulated transition rate per photon per mode, V_a is the volume of the mode in the active medium, τ is the lifetime of the upper laser level, τ_c is the photon lifetime.

Substituting these two groups of equations we obtain:

$$\frac{d\delta N}{dt} = -\delta N\left(B\phi_0 + \frac{1}{\tau}\right) - BN_0\delta\phi; \tag{3.5}$$

$$\frac{d\delta\phi}{dt} = BV_a\phi_0\delta N; \tag{3.6}$$

Substitution of Eq. 3.5 into Eq. 3.6 gives

$$\frac{d^2\delta\phi}{dt^2} + \left(B\phi_0 + \frac{1}{\tau}\right)\frac{d\delta\phi}{dt} + \left(B^2V_aN_0\phi_0\right)\delta\phi = 0. \tag{3.7}$$

The solution will look as:

$$\delta\phi = \delta\phi_0 \exp(pt), \tag{3.8}$$

$$p = -\frac{1}{t_0} \pm \left[\frac{1}{t_0^2} - \omega^2\right]^{1/2}, \tag{3.9}$$

$$\omega^2 = B^2 V_a N_0 \phi_0, \tag{3.10}$$

$$t_0 = 2\left[B\phi_0 + \frac{1}{\tau}\right]^{-1}. \tag{3.11}$$

In the condition $t_0 \leq \omega^{-1}$ the two solutions for p given by Eq. 3.9 are both real and negative. In this case the time behavior of $\delta\phi(t)$ (Eq. 3.8) consists of a superposition of two exponentially damped decays. The second case is where $t_0 > \omega^{-1}$. In this case, from Eq. 3.8 $\delta\phi(t)$ is shown to correspond to a damped sinusoidal oscillation:

$$\delta\phi = C \exp\left(-\frac{t}{t_0}\right) \sin(\omega t + \beta) \tag{3.12}$$

where C and β are provided by the initial conditions. In this case the oscillation period is determined by the geometric mean of τ and the photon lifetime τ_c, whereas the damping time t_0 of the oscillation is determined by the upper state lifetime.

The condition $t_0 \leq \omega^{-1}$ could be observed when $(\tau_c/\tau) > 4(x-1)/x^2$, where $x = R_p/R_{cp}$ is the amount by which the threshold is exceeded. If $\tau_c > \tau$, this condition is always satisfied for any value of x. This situation usually occurs in gas lasers, which therefore generally do not exhibit spiking behavior.

These simple results appear to conflict with many experimental results, which indicated that many lasers, even CW ones, tend to exhibit a continuous pulsating behaviour, sometimes irregular and sometimes regular. It can be seen that the output consists of a train of pulses irregularly spaced in time and of random amplitude (irregular spiking). In single-mode lasers, one of the main causes of instability arises from an external and usually accidental modulation of pump rate or cavity losses. For a random modulation, this simply leads to a higher laser noise intensity.

In multimode lasers, a new type of instability may easily set in, due to, for example, a pump modulation-induced switching in time between one mode and another or from one set of modes to another set. This instability leads to a kind of antiphase motion (antiphase dynamics) among the modes and it can be adequately described by a rate equation treatment in which, for a homogeneous line, the cross saturation effect due to spatial hole burning is taken into account.

To summarize, we can say that single mode lasers do not usually exhibit dynamical instability, but instead, show some, possibly quite pronounced, intensity noise due to unavoidable perturbations of laser parameters. On the other hand, multimode lasers may also present additional instabilities due to a kind of antiphase motion among the oscillating modes. Depending on the amplitude of modulation of the laser parameters, on the type of laser, and on whether the line is homogeneously or inhomogeneously broadened, this instability may lead either to a mode partition noise or even to strong laser pulsations.

3.3 Q-switching

We have seen in the previous chapter that in a CW operation, the population inversion gets clamped to its threshold value when the oscillation starts. Even under the pulsed operating conditions, the population inversion can only exceed the threshold value by a relatively small amount due to the onset of stimulated emission. Suppose now that a shutter is introduced into the laser cavity. If the shutter is closed, the laser action is prevented and the population inversion can then reach a value far exceeding the threshold population for the case where is no shutter. If the shutter is now opened suddenly, the laser will exhibit a gain that greatly exceeds losses and the stored energy will be released in the form of a short and intense light pulse. Since this operation involves switching the cavity Q factor from a low to a high value, the technique is usually called Q-switching. It allows the generation of laser pulses of duration comparable to the photon decay time (i.e. from a few nanoseconds to a few dozens of nanoseconds) and a high peak power (in the megawatt range).

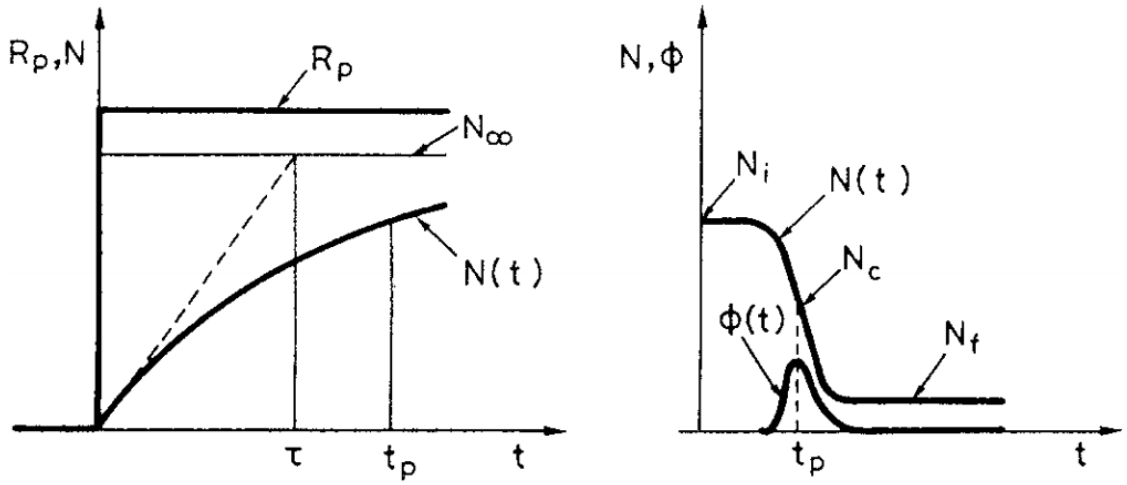

Figure 3.2: Example of the temporal behavior of the total inversion, $V_a N(t)$, and photon number, $\phi(t)$, for a three-level laser.

In order to describe the Q-switching dynamical behavior, we assume that a step pump pulse is applied to a laser starting at time $t = 0$, $R_p(t) = 0$ for $t < 0$ and $R_p(t) = R_p = const$ for $0 < t < t_p$ and that, meanwhile, the shutter is closed. For $0 < t < t_p$ the time behavior of the population inversion can then be calculated by the equation:

$$N(t) = N_\infty \left[1 - exp\left(\frac{-t}{\tau}\right)\right] \tag{3.13}$$

where $N_\infty = R_p \tau$. The time behavior of $N(t)$ is also shown in Fig. 3.2. We can see that the duration t_p of the pump pulse is ideally to be similar to or shorter than the upper state

lifetime τ. In fact, for $\tau_p \ll \tau$, $N(t)$ would not undergo any appreciable increase and the pump power, rather than being accumulated as inversion energy, would be wasted through spontaneous decay. To achieve a sufficiently large inversion, a long lifetime τ is essential. Thus, Q-switching can be used effectively with electric-dipole forbidden laser transitions that generally fall in the millisecond range. This is the case of most solid-state lasers (e.g., Nd, Yb, Er, Ho) in various host materials, Cr doped materials such as alexandrite, Cr:LISAF, and ruby) and some gas lasers (e.g. CO_2 or iodine). On the other hand, for semiconductor lasers, dye lasers, and a number of important gas lasers (e.g., He-Ne, Ar, Excimers) a laser transition is electric-dipole allowed and the lifetime is of the order of a few to a few dozen of nanoseconds. In this case, with the usual values of pump rates, R_p, available, the achievable inversion N_∞ is too low to be of interest for Q-switching.

There are several methods that have been developed to achieve switching the cavity, and the most commonly used are electro-optical shutters, rotating prisms, acousto-optical switches, and saturable absorbers. These devices are generally classified into two categories, the active and the passive Q-switches. In an active Q-switching device, one must apply some external active operation to this device (e.g. change the voltage applied to the electro-optical shutter) to produce Q-switching. In a passive Q-switch, the switching operation is automatically produced by optical nonlinearity of the element used (e.g. saturable absorber).

Electro-optical Q-switching devices make use of a cell exploiting the electro-optical effect, usually the Pockels effect, to induce the Q-switching. A cell based on the Pockels effect (Pockels cell) consists of a proper nonlinear crystal, such as KD*P or lithium niobate for the visible-to-near-infrared region in which an applied DC voltage induces a change in the crystal's refractive indices. This induced birefringence is proportional to the applied voltage. Pockels cell Q-switches are very widely used. Depending upon the particular nonlinear crystal used in the cell, the particular arrangement of the applied field, the crystal dimensions, and the value of the wavelength involved, the $\lambda/4$ voltage may range between 1 and 5 kV. This voltage must then be switched off after the time t_s, smaller than the build-up time of the Q-switched pulse (typically $t_s < 20$ ns).

The most common mechanical means of Q-switching involves rotating one of the end mirrors of the laser resonator about an axis perpendicular to the resonator axis. In this case, the high-Q condition is reached when the rotating mirror passes through a position parallel to the other cavity mirror. To simplify the alignment requirements, a 90° roof-top prism with the roof edge perpendicular to the rotation axis is often used instead of an ordinary mirror. Such a prism has the property that, for the light propagating orthogonally to the roof edge, the reflected beam is always parallel to the incident beam regardless of any rotation of the prism about its roof edge. This ensures that the alignment between the prism and the other cavity mirror is always achieved in the plane orthogonal to the roof. The effect of rotation is then to align the prism in the other direction. Typically the duration of the high Q-switching condition is about 400 ns, this slow switching time can sometimes result in the production of multiple pulses.

An acousto-optic modulator consists of a block of transparent optical material (e.g., fused quartz in the visible to near-infrared and germanium or cadmium selenide in the

middle-far infrared) in which an ultrasonic wave is launched by a piezoelectric transducer bonded to one side of the block and driven by a radiofrequency oscillator. The side of the block opposite to the transducer side is cut off at an angle and has an absorber for the acoustic wave placed on its surface. With a back reflection of the acoustic wave thus suppressed, only a travelling acoustic wave is present in the medium. The strain induced by the ultrasonic wave results in local changes of the material refractive index through photoelastic effect. This periodic change of refractive index acts then as a phase grating with a period equal to the acoustic wavelength, the amplitude proportional to the sound amplitude, and which is travelling at the speed of sound in the medium (travelling-wave phase grating). Its effect is to diffract a fraction of the incident beam out of the incident beam direction. Thus, if an acousto-optic cell is inserted in the laser cavity, there will be an additional loss present, due to the beam diffraction, when the driving voltage to the transducer is applied. If the driving voltage is high enough, this additional loss will be sufficient to prevent the laser from oscillating. The laser is then returned to its high-Q condition by switching off the transducer voltage. Acousto-optic modulators have the advantage of low optical insertion losses, and, for repetitive Q-switching, they can readily be driven at high repetition rates (kHz). The loss involved in the low-Q situation is rather limited, however, and the Q-switching time is rather long (mainly resulting from the time taken for an acoustic wavefront to traverse the laser beam). These modulators are therefore used, primarily, for repetitive Q-switching of low-gain CW-pumped lasers (e.g. Nd:YAG).

3.4 Mode-Locking

Let us now consider a laser that is oscillating in a rather large number of longitudinal modes. Under ordinary circumstances, the phases of these modes will have random values and, for CW oscillation, the beam intensity will show a random time behaviour. Let us now suppose that the oscillating modes, while having equal or similar amplitudes, are somehow made to oscillate with some relation between their phases. Such a laser is referred to as mode-locked, and the process by which the modes are made to adopt a definite phase relation is referred to as mode-locking.

3.4.1 Frequency-Domain Description

First, we will describe mode-locking in the frequency domain and consider, as the first example, the case of $2n + 1$ longitudinal modes oscillating with the same amplitude E_0. We will assume the phases φ_l of the modes in the output beam to be locked according to the relation $\varphi_l - \varphi_{l-1} = \varphi$, where φ is a constant. The total electric field $E(t)$ of the e.m.

wave, at any given point in the output beam, can be written as:

$$E(t) = \sum_{-n}^{+n} E_0 \exp\{j\left[(\omega_0 + l\Delta\omega)\, t + l\varphi\right]\}, \tag{3.14}$$

where ω_0 is the frequency of the central mode, $\Delta\omega$ is the frequency difference between two consecutive modes, and where the value of the phase for the central mode has, for simplicity, been taken to be zero. Equation 3.14 could be simplified to the system:

$$E(t) = A(t) \exp\left(j\omega_0 t\right), \tag{3.15}$$

$$A(t) = \sum_{-n}^{+n} E_0 \exp\left[jl\left(\Delta\omega t + \varphi\right)\right]. \tag{3.16}$$

Equation 3.15 shows that $E(t)$ can be represented in terms of a sinusoidal carrier wave, at the center-mode frequency ω_0, whose amplitude $A(t)$ is time dependent. To calculate the time behavior of $A(t)$, we now change to a new time reference t' such that $\Delta\omega t' = \Delta\omega t + \varphi$. In terms of the new variable t', Eq. 3.16 transforms to:

$$A(t) = \sum_{-n}^{+n} {}_l E_0 \exp\left(jl\Delta\omega t'\right) \tag{3.17}$$

and the sum appearing on the right-hand side can be easily recognized as a geometric progression with a ratio $\exp(jl\Delta\omega t')$ between consecutive terms. Summation of this progression can then be easily performed and we obtain:

$$A(t') = E_0 \frac{\sin\left[(2n+1)\,\Delta\omega t'/2\right]}{\sin\left[\Delta\omega t'/2\right]} \tag{3.18}$$

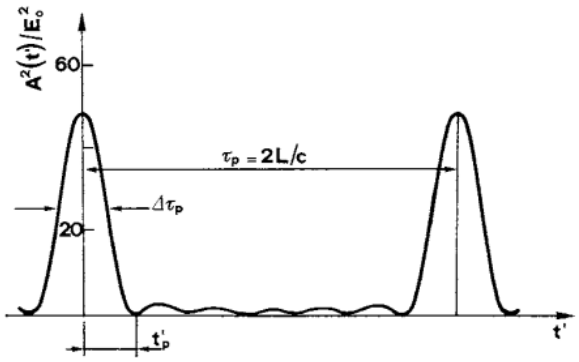

Figure 3.3: Time behavior of the squared amplitude of the electric field for the case of seven oscillating modes with locked phases and equal amplitudes, E_0.

To help understand the physical significance of this expression, Fig. 3.3 shows the quantity $A^2(t')/E_0^2$, $A^2(r')$ being proportional to the beam intensity, versus time t_0, for

2n+1=7 oscillating modes. It is shown that, as a result of the phase-locking condition, the oscillating modes interfere so as to produce a train of evenly spaced light pulses. The pulse maxima occur at those times for which the denominator of Eq. 3.18 vanishes. In the new time reference $t^{'}$, the first maximum occurs for $t^{'}$=0. Note that, this time, the numerator of Eq. 3.18 also vanishes and, after the approximation $sin\ \alpha \cong \alpha$, which holds for small values of α, we readily see from Eq. 3.18 that $A^2(0) = (2n+1)^2 E_0^2$. The next pulse will occur when the denominator of Eq. 3.18 vanishes again and this will happen at the time $t^{'}$ so that $(\triangle\omega t^{'}/2) = \pi$. Two successive pulses are therefore separated by certain time:

$$\tau_p = 2\pi/\triangle\omega = 1/\triangle\nu, \tag{3.19}$$

where $\triangle\nu$ is the frequency separation between two consecutive oscillating modes. For $t^{'} > 0$, the first zero for $A^2(t^{'})$ in Fig. 3.3 occurs when the numerator of Eq. 3.18 vanishes again. This occurs at the time $t_p^{'}$ so that $[(2n+1)\triangle\omega t_p^{'}/2] = \pi$. Since the width $\triangle t_p$ (FWHM) of $A^2(t^{'})$, i.e. of each laser pulse, is approximately equal to $t_p^{'}$, we thus have:

$$\triangle\tau_p \cong 2\pi/(2n+1)\triangle\omega = 1/\triangle\nu_L, \tag{3.20}$$

where $\triangle\nu_L = (2n+1)\triangle\omega/2\pi$ is the total oscillating bandwidth.

3.4.2 Methods of Mode-Locking

Methods of mode-locking, like those of Q-switching, can be classified into two categories: (1) Active-mode-locking, in which the mode-locking element is driven by an external source. (2) Passive mode-locking, in which the element which induces mode-locking is not driven externally and instead, exploits a nonlinear optical effect such as the saturation of a saturable absorber or nonlinear refractive index change of a suitable material.

3.4.3 Active Mode-Locking

There are three main types of active mode-locking (ML), namely: (1) Mode-locking induced by an amplitude modulator (AM mode-locking); (2) Mode-locking induced by a phase modulator (FM mode-locking); (3) Mode-locking induced by a periodic modulation of the laser gain at a repetition rate equal to the fundamental cavity frequency $\triangle\nu = c/2L$ (ML by synchronous pumping). We will discuss AM mode-locking in most detail, this type being the most popular, and then give a brief discussion of the FM mode-locking. Mode-locking by synchronous pumping will not be discussed here as it is seldom used. In fact, it only applies to active media with nanosecond relaxation time, namely, dye media, and, to obtain the shortest pulses, requires that the modulation rate of the pump be equal, within high precision, to the fundamental frequency of the laser cavity. For this reason, pulse durations shorter than 1 ps are difficult to achieve from a synchronously pumped dye laser.

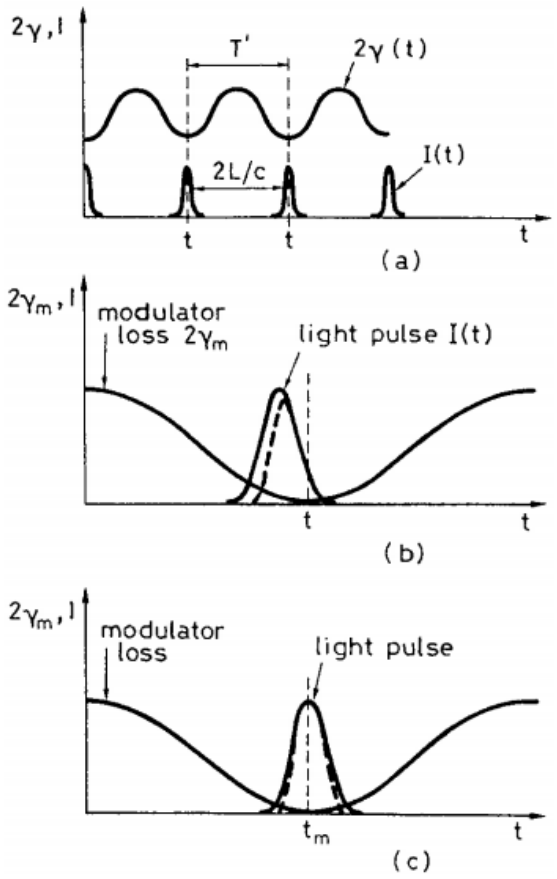

Figure 3.4: Time-domain description of AM mode-locking: (a) steady state condition; (b) light pulse arriving before the time t_m of the minimum loss; (c) pulse-shortening occurring when the pulse arrives at time t_m.

To describe AM-mode-locking, we suppose a modulator to be inserted in the cavity, which produces a time-varying loss at frequency ω_m. If $\omega_m \neq \triangle\omega$, where $\triangle\omega = 2\pi\triangle\nu$, $\triangle\nu$ being the frequency difference between longitudinal modes, this loss will simply amplitude modulate the electric field, $E_l(t)$, of each cavity mode to give:

$$E_l(t) = E_0[1 - (\delta/2)(1 - cos\omega_m t)]cos(\omega_l t + \phi_l), \tag{3.21}$$

where ω_l is the mode frequency, ϕ_l its phase and where δ is the depth of the amplitude modulation, which means that the field amplitude is modulated from E_0 to $E_0(1-\delta)$. Note that the term $E_0(\delta/2)cos\omega_m t \times cos(\omega_l t+\phi_l)$ in Eq. 3.21 can be written as $(E_0\delta/4)(cos[(\omega_l+\omega_m)t + \phi_l] + cos(\omega_l - \omega_m)t + \phi_l])$. Thus, $E_l(t)$ actually contains two terms oscillating at the frequencies $\omega_l \pm \omega_m$ (modulation side-bands). If now $\omega_m = \triangle\omega$, these modulation side-bands will coincide with the adjacent mode frequencies of the resonator. These two side-bands will thus contribute to the field equations of the two adjacent cavity modes. So, the equations for cavity modes become coupled i.e., the field equation of a given cavity

mode will contain two contributions arising from the modulation of the adjacent modes.

The details of the operation of AM mode-locking can be more readily understood in the time domain rather than in the frequency domain. Thus, Fig. 3.4 shows the time behavior of the cavity round-trip power losses 2γ which are modulated with a modulation period $T = 2\pi/\omega_m$. We will assume the modulator to be placed at one end of the cavity. If now $\omega_m = \triangle\omega$, the modulation period T will be equal to the cavity round-trip time and the stable steady-state condition will correspond to light pulses passing through the modulator at the times t_m when a minimum loss of the modulator occurs Fig. 3.4a. Indeed, if a pulse is assumed to pass through the modulator at a time of minimum loss, it will return to the modulator after a time, 2L=c, where the loss is again at a minimum.

To describe FM mode-locking, we suppose a modulator, whose refractive index n is sinusoidally modulated at frequency ω_m, to be inserted at one end of the cavity. Any given mode of the cavity will therefore be subjected to a time-varying phase shift given by $\phi = (2\pi L^{'}/\lambda) \times n(t)$, where $L^{'}$ is the modulator length. These phase-modulated modes will show sidebands whose frequencies, for $\omega_m = \triangle\omega$, coincide with those of the neighbouring modes. Thus, the cavity modes become coupled again and their phases are locked. In the time domain, this FM mode-locking produces pulses as indicated in Fig. 3.5. In this case, two stable mode-locking states can occur, i.e., namely, when the light pulse passes through the modulator either at each minimum of $n(t)$ (solid-line pulses) or each maximum (dotted-line pulses). To get some physical understanding of what happens in this case, we first observe that, since the optical length of the modulator is $L^{'}{}_e = n(t)L^{'}$, this type of modulation results in the modulation of the overall optical length, L_e, of the cavity. The cavity is thus equivalent to one without a modulator but where the position of one cavity mirror is oscillating at frequency ω_m. Each of the two stationary situations of Fig. 3.5 thus corresponds to mode-locked pulses striking this moving mirror when it is at either of its extreme positions (i.e., when the mirror is stationary).

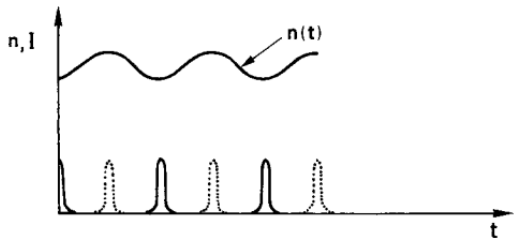

Figure 3.5: FM mode-locking. Time behavior of modulator refractive index n and of output intensity I.

For a pulsed and generally high gain laser, AM mode-locking is commonly achieved by a Pockels cell amplitude modulator. For a CW pumped and generally low gain laser, AM mode-locking is more commonly achieved with an acousto-optic modulator, owing to its lower insertion loss compared to a Pockels cell modulator. In fact, the face to which the piezoelectric transducer is bonded and the opposite one of the optical material are

now cut off parallel to each other. The sound wave launched into the material by the transducer is then reflected back by the opposite face of the material.

3.4.4 Passive Mode-Locking

There are four main types of passive mode-locking (ML), namely: (1) fast saturable absorber ML, which makes use of the saturation properties of a suitable absorber (e.g. a dye molecule or a semiconductor) with a very short upper state lifetime; (2) Kerr Lens Mode-locking (KLM), which exploits the self-focusing property of a suitable transparent nonlinear optical material; (3) Slow saturable absorber ML, which exploits the dynamic saturation of the gain medium; (4) Additive Pulse ML (APM), in which one exploits the self-phase-modulation induced in a suitable non-linear optical element inserted in an auxiliary cavity, coupled to the main cavity and of the same length. In the latter case, the pulse shortening mechanism arises from the interference of the main pulse in the laser cavity with the pulse which is coupled back from the auxiliary cavity and which has been phase modulated by the nonlinear material. However, APM locking requires that the optical lengths of the two cavities should be equal with a typical accuracy of a fraction of the laser wavelength. For this reason, this type of ML is not so widely used as the other techniques and will not be discussed further here.

To illustrate mode-locking by a fast saturable absorber, we consider an absorber with low saturation intensity and with relaxation time much shorter than the duration of the mode-locked pulses. For low values of intracavity beam intensity, I, compared to the absorber's saturation intensity, I_s, the cavity round trip power loss can be written as:

$$2\gamma_t = 2\gamma_t - 2\gamma^{'}(I/I_s) \tag{3.22}$$

Another fast passive mode-locking technique relies on the lens-effect induced in a suitable material by a Kerr-type non-linearity and is thus referred to as Kerr-Lens-ModeLocking (KLM). Consider first an optical material, such as quartz or sapphire, traversed by a light beam of uniform intensity I. At a properly high intensity, the refractive index of the medium will be influenced to a readily observable extent by the field intensity, i.e., one can generally write $n = n(I)$. The first term of a Taylor expansion of n vs I will be proportional to I, and n can thus be written as:

$$n = n_0 + n_2 I, \tag{3.23}$$

where n_2 is the positive coefficient which depends on the material (e.g. $n_2 \cong 4.5 \times 10^{-}16\ cm^2/W$ for fused quartz and $n_2 \cong 3.45 \times 10^{-}16\ cm^2/W$ for sapphire). This phenomenon is known as optical Kerr effect and is generally due to a hyperpolarizability of the medium occurring at high electric fields and arising from either a deformation of the electronic orbitals of atoms or molecules or from a reorientation of the molecules (for a gas or a liquid).

For a solid, only a deformation of the atom's electron cloud can occur and optical Kerr effect is very fast, the response time being of the order of a rotation period of the outermost

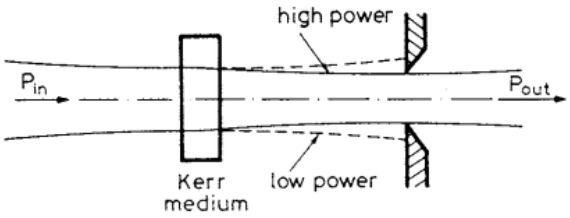

Figure 3.6: Non-linear loss element exploiting optical Kerr effect in a suitable non-linear material.

electrons of the atom (a few femtoseconds). Assume now that the beam intensity, in a medium exhibiting the optical Kerr effect (a Kerr medium), has a given transverse profile, e.g., Gaussian. The intensity at the beam centre will then be larger than in the wings and, according to Eq. 3.23, a nonlinear refractive index change, $\delta n = n_2 I$, will be induced, which is positive at the beam centre and reaches to zero in the wings of the beam. For a Gaussian beam profile, i.e., $I = I_p exp - 2(r/w)^2$, where I_p is the peak intensity and w is the (field) spot size, the non-linear phase shift acquired by the beam when traversing a length l of the medium will be $\delta\phi = 2\pi\delta n l/\lambda = (2\pi n_2 I_p l/\lambda) exp - 2(r/w)^2 \cong (2\pi n_2 I_p l/\lambda) \times [1 - 2(r/w)^2]$. Thus, to first order in $(r/w)^2$, $\delta\phi$ can be taken as a parabolic function of (r/w), which amount to a spherical lens being induced in the medium by the optical Kerr effect. In fact, this induced lens may lead to beam focusing when the beam power exceeds a critical value, the phenomenon known as self-focusing. A nonlinear loss element providing a loss of the general form of Eq. 3.22 can then be implemented as shown schematically in Fig. 3.6. In fact, at higher beam intensities, the beam will be focused more strongly at the aperture and, therefore, less loss will be experienced at that aperture. In fact, the time response of KLM is very short, so that, for all practical purposes, it can be taken to be instantaneous. By appropriate control of cavity dispersion, the fastest ML pulses have been achieved by this technique using ultra-broadband gain media (bandwidths of ≈ 100 THz).

Although many passively mode-locked lasers that use fast saturable absorbers, slow saturable absorbers can also lead to mode-locking and this type of ML is often referred to as slow-saturable-absorber ML. The special circumstances required can be summarized as follows: (i) the relaxation time of both the absorber and the amplifier must be comparable to the cavity round trip time; (ii) the saturation fluence of both the gain medium [$\Gamma_{sg} = h\nu/\sigma_g$] and the saturable absorber [$\Gamma_{sa} = h\nu/2\sigma_a$] must be low enough to allow both media be saturated by the intracavity laser fluence; (iii) the saturation fluence of the gain medium must be comparable to, although somewhat larger than that of the saturable absorber.

The physical phenomena that lead to mode-locking, in this case, are rather subtle and will be described with the help of Fig. 3.7, where, for simplicity, it is supposed that both the saturable absorbers and the active medium are together at one end of the cavity. Before the arrival of the mode-locked pulse, the gain is assumed to be smaller than the

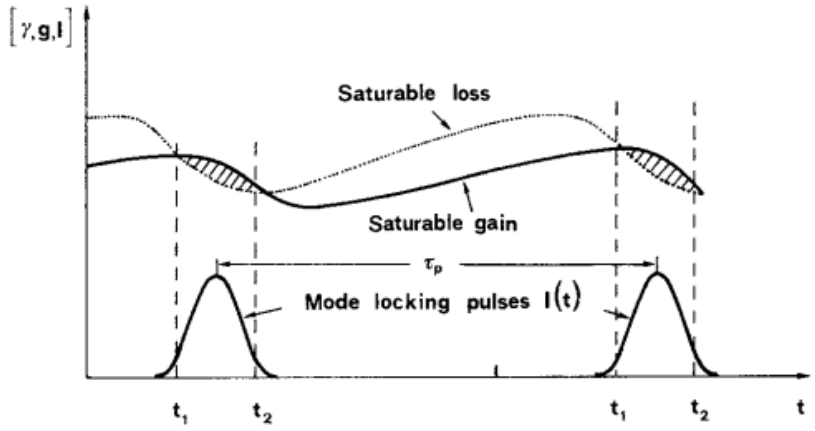

Figure 3.7: Time-domain picture of slow-saturable-absorber mode-locking. Note that the figure is not to scale since the time duration of a mode-locked pulse is typically in the hundreds femtosecond range while the time interval τ_p between two consecutive pulses, i.e., the cavity round trip time is typically a few nanoseconds.

losses, so that the early part of the leading edge of the pulse will suffer a net loss. If the total energy fluence of the pulse has a proper value, the accumulated energy fluence of the pulse may become comparable to the saturation fluence of the absorber during the leading edge of the pulse. Saturation of the saturable absorber will begin to occur so that, at some time during the pulse leading edge (time t_1 in Fig. 3.7), the absorber loss becomes equal to the laser gain. For $t > t_1$ the pulse will then experience a net gain rather than a net loss. However, if the saturation energy fluence of the gain medium has a proper value (typically twice as high as that of the absorber), gain saturation will be produced so that, at some time during the trailing edge of the pulse (time t_2 in Fig. 3.7), the saturated gain becomes equal to the saturated loss. For $t > t_2$ the pulse will then again experience see a net loss rather than a net gain, and a time window of the net gain will thus be established for $t_1 < t < t_2$. Thus, after each pass through the absorber-amplifier combination, the pulse is shortened and a steady-state condition is again established by the balance between this pulse shortening mechanism and the pulse broadening arising from the finite gain bandwidth. The pulse duration is thus again expected to be comparable the inverse of the gain bandwidth $\triangle\nu_0$.

A large number of various lasers have been designed to operate mode-locked, both actively and passively, including many gas lasers (e.g., He-Ne, Ar ion and CO_2 lasers), all of the commonly used solid-state lasers, many semiconductor lasers and many dye lasers. As some representative examples, Table 3.1 shows the most common media providing picosecond and femtosecond laser pulses, in CW ML, together with the corresponding values of the gain linewidth $\triangle\nu_0$, the peak stimulated emission cross-section σ, and the upper state lifetime τ. In the same table, the shortest pulse duration, τ_p, so far achieved and the minimum pulse duration, $\triangle\tau_{mp} = 0.44/\triangle\nu_0$, achievable from a particular laser are also shown. One should remember that the threshold pump power is inversely proportional

to $\sigma\tau$. Thus, for a given gain medium, $1/\sigma\tau$ can be taken as a figure of merit for achieving the lowest threshold while $1/\triangle\nu_0$ represents a figure of merit to produce the shortest pulses.

Laser medium	$\Delta\nu_0$	$\sigma[10^{-20}\,\mathrm{cm}^2]$	$\tau[\mu\mathrm{s}]$	$\Delta\tau_p$	$\Delta\tau_{mp}$
Nd:YAG $\lambda = 1.064\,\mu\mathrm{m}$	135 GHz	28	230	5 ps	3.3 ps
Nd:YLF $\lambda = 1.047\,\mu\mathrm{m}$	390 GHz	19	450	2 ps	1.1 ps
Nd:YVO_4 $\lambda = 1.064\,\mu\mathrm{m}$	338 GHz	76	98	<10 ps	1.3 ps
Nd:glass $\lambda = 1.054\,\mu\mathrm{m}$	8 THz	4.1	350	60 fs	55 fs
Rhodamine 6G $\lambda = 570\,\mathrm{nm}$	45 THz	2×10^4	5×10^{-3}	27 fs	10 fs
Cr:LISAF $\lambda = 850\,\mathrm{nm}$	57 THz	4.8	67	18 fs	8 fs
Ti:sapphire	100 THz	38	3.9	6–8 fs	4.4 fs

Table 3.1: Most common media providing picosecond and femtosecond laser pulses together with the corresponding values of: (a) the gain linewidth, $\triangle\nu_0$; (b) the peak stimulated emission cross-section, δ; (c) the upper state lifetime, τ; (d) the shortest pulse duration so far reported, $\triangle\tau_p$; (e) the shortest pulse duration, $\triangle\tau_{mp}$, achievable from the same laser

Questions

1. What is the essence of the Q-switching technique?
2. What is the difference between passive and active mode-locking?
3. Estimate changing of refractive index in silica glass with nonlinear index $n_2 = 2.4 \cdot 10^{-20}$ m^2/W for pulse with energy 10 μJ, diameter 1 mm and pulse duration 100 fs.

References

1. Svelto O., Hanna D. C. Principles of lasers. – New York : Plenum press, 1998. – V. 4.
2. Diels J. C., Rudolph W. Ultrashort laser pulse phenomena. – Elsevier, 2006.

Chapter 4

Micro- and nanolasers

4.1 Vertical-cavity surface-emitting lasers

Vertical-cavity surface-emitting lasers (VCSELs) represent one of the most commonly used types of microlasers invented many years after the initial demonstration of a conventional edge-emitting laser (EEL). VCSELs offer a reduction of size of at least an order of magnitude in the overall device volume compared to EELs (see Fig. 4.1). Currently, VCSELs are among the most energy-efficient types of lasers commercially applied. However, VCSELs with energy efficiency as high as 50 fJ/bit have been demonstrated only in research laboratories, and those commercially available have a much lower energy efficiency.

Typical VCSELs have diameters from 2 μm to 10 μm with a total distributed Bragg reflector (DBR) thickness from 5 μm to 10 μm, resulting in the overall device volume of 10 to 100 times larger the λ^3, although the modal volumes are much smaller. Any further significant reduction in sizes and energy usage is challenging due to poor heat dissipation through thick DBR mirrors and poor lateral confinement of the VCSEL structures. Thus, it is very difficult for VCSELs to meet long-term requirements on laser size and energy efficiency for on-chip applications despite their important improvement in recent years.

4.2 Microdisk lasers

Microdisk lasers were initially developed in an attempt to miniaturize semiconductor lasers for integrated photonics applications using a free-standing piece of semiconductor supporting the whispering-gallery modes due to the high contrast of refractive indices between the semiconductor and the air. Such high index contrast provides the strongest mode confinement practically possible without using metals or thick DBRs. This unique development provided much smaller lasers than any of those available at the time. The initial devices had diameters between 3 μm and 5 μm, with a thickness of approximately

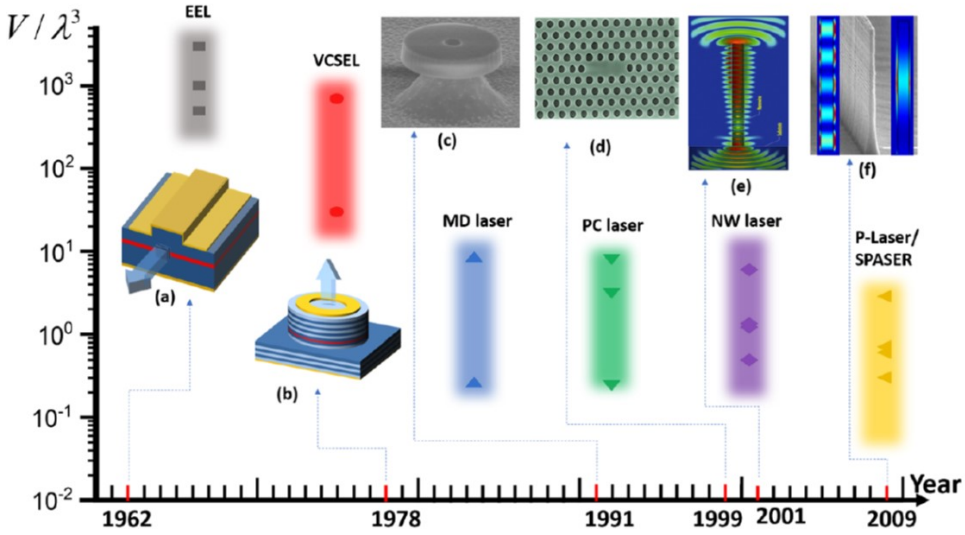

Figure 4.1: Device volume normalized by the λ^3 for several types of semiconductor lasers: EEL, edge-emitting laser; VCSEL, vertical-cavity surface-emitting laser; MD, microdisk lasers; PC laser, photonic crystal; NW laser, nanowire laser; P-laser/SPASER, plasmonic lasers. The colored bars indicate the ranges of values found in the references. The red marks along the x axis indicate the year when each laser was first experimentally demonstrated. The yellow bar is intentionally extended downward beyond the data symbols to indicate the potential for a further size reduction of plasmonic lasers and spasers. [1]

1 μm, resulting in the overall device volume several times large than λ^3. In a recent work [2] [3], combining a photonic crystal (PC) structure with a microdisk allowed a total device volume of only a small fraction of the λ^3, which is one of the smallest total volumes achieved (see Fig. 4.1). Significant progress has also been recently demonstrated in perovskite micro- and nano-disk lasers. Perovskites show remarkable optoelectronic properties and may find many interesting applications in the domains, however, their use for on-chip interconnects is hindered by several issues such as incompatibility with traditional microfabrication and the lack of perovskites emitting at near-infrared communication wavelengths (e.g., $> 850\ nm$).

4.3 Nanowire lasers

Semiconductor nanowires NWs, or nanopillars, provide one of the best semiconductor optical cavities in air due to the high index contrast (similar to that of microdisk lasers). Again, similar to the microdisk lasers, the mode confinement in nanowires is much better than that in typical double heterostructures, with the possibility of achieving a

confinement factor of > 1. Such nanowires with both ends in air are unique both as a high-reflective laser cavity and as a gain medium, and this is an ideal combination for laser miniaturization. With the initial NW lasers working in the UV and visible ranges, the near IR lasing was then first demonstrated using a single GaSb nanowire at the telecom wavelengths. Recently, several NW lasers were implemented in the short-wavelength NIR range. To date, almost all of these NWs have shown lasing under optical pumping, with only one exception. The volumes of nanowire lasers are currently comparable to those of microdisk lasers and photonic crystal lasers (see Fig. 4.1), with the overall size as small as twice the λ^3 in the IR range.

Further miniaturization of nanowires is also possible. An additional advantage of NW lasers is the use of combined materials and bandgap flexibility, which allows the implementing of lasers at the wavelengths that are difficult to achieve with microdisk and photonic crystals lasers.

4.4 Laser rate equations and β-factor

The rate equations are a standard and a widely used method for investigating both steady-state and dynamical behaviour of a laser. For nanolasers, however, extra care is needed. For example, the Purcell effect, which characterizes the change of the spontaneous emission rate in a subwavelength cavity compared to that in free space, has to be incorporated into the rate equations; the optical field has to be properly normalized; the dispersion of materials has also to be considered, especially for metals.

Considering these factors and the dependence of the carrier density on various parameters, the rate equations can be written as:

$$\frac{\partial n}{\partial t} = \eta_i \frac{I}{qV_a} - R_{nr}(n) - R_{sp}(n) - R_{st}(n)S, \tag{4.1}$$

$$\frac{\partial S}{\partial t} = -\frac{S}{\tau_p} + \Gamma_E \beta(n) R_{sp}(n) + \Gamma_E R_{st}(n)S, \tag{4.2}$$

where n is the carrier density, I is the injection current, η_i is the current injection efficiency, q is the electron charge, V_a is the active volume, $R_{nr}(n)$ is the non-radiative recombination rate, $R_{sp}(n)$ is the total spontaneous emission rate, $R_{st}(n)$ is the stimulated emission coefficient, S is the photon density, $\beta(n)$ is the spontaneous emission coupling factor, τ_p is the photon lifetime, and Γ_E is the energy confinement factor.

In different versions of rate equations, the confinement factor Γ is referred to as power confinement, electric field confinement, electric energy confinement, and total

optical energy confinement. The non-radiative recombination consists of trap-assisted recombination that dominates below the lasing threshold and Auger recombination that dominates far above the threshold, which can be written as:

$$R_{nr} = An + Cn^3, \tag{4.3}$$

where A is the non-radiative recombination coefficient and C is the Auger recombination coefficient.

The photon lifetime τ_p is related to the mode wavelength and to the Q factor as:

$$\frac{1}{\tau_p} = \frac{\omega_k}{Q}, \tag{4.4}$$

where ω_k is the resonant angular frequency of the k-th mode. The total spontaneous emission rate $R_{sp}(n)$ includes spontaneous emission from all discrete cavity modes, in addition to the radiation into the free space continuum of modes. It is expressed as:

$$R_{sp}(n) = \sum_{k=1} R_{sp,k}(n) + \sum_{k\neq 1} R_{sp,k}(n) + \frac{1}{\tau_{sp,rad}} \int d\mathrm{K} f_{c,\mathrm{K}} \left(1 - f_{v,\mathrm{K}}\right), \tag{4.5}$$

where $k = 1$ denotes the lasing mode, and $k \neq 1$ denotes all other cavity modes. The last term in Eq. 4.5 describes the radiation into the free-space continuum of modes, and it is written as the ratio of the carrier recombination involving the density of states available in the active medium to spontaneous radiative lifetime $\tau_{sp,rad}$. Finally, the single-mode spontaneous emission rate $R_{sp,k}(n)$ is related to the total spontaneous emission rate $R_{sp}(n)$ as:

$$R_{sp,k}(n) = \beta(n) \cdot R_{sp}(n). \tag{4.6}$$

In Eq. 4.6, the carrier density dependency of β results from the Purcell factor, which is pump-dependent: it grows with the increasing carrier density, until the threshold condition is reached. In the related papers, however, the β-factor is usually considered independent of the carrier density. The cavity Purcell factor F_p is defined as the ratio of spontaneous emission in a cavity to that in free space:

$$F_p \equiv \frac{\tau_{bulk}}{\tau_{cav}} \approx \left[\frac{3}{4\pi^2} \frac{Q}{V_a} \left(\frac{\lambda}{n} \right)^3 \right]. \tag{4.7}$$

F_p can be large in small laser cavities due to its inverse proportionality to the active-region volume V_a. However, F_p is inversely proportional to the effective size of the mode

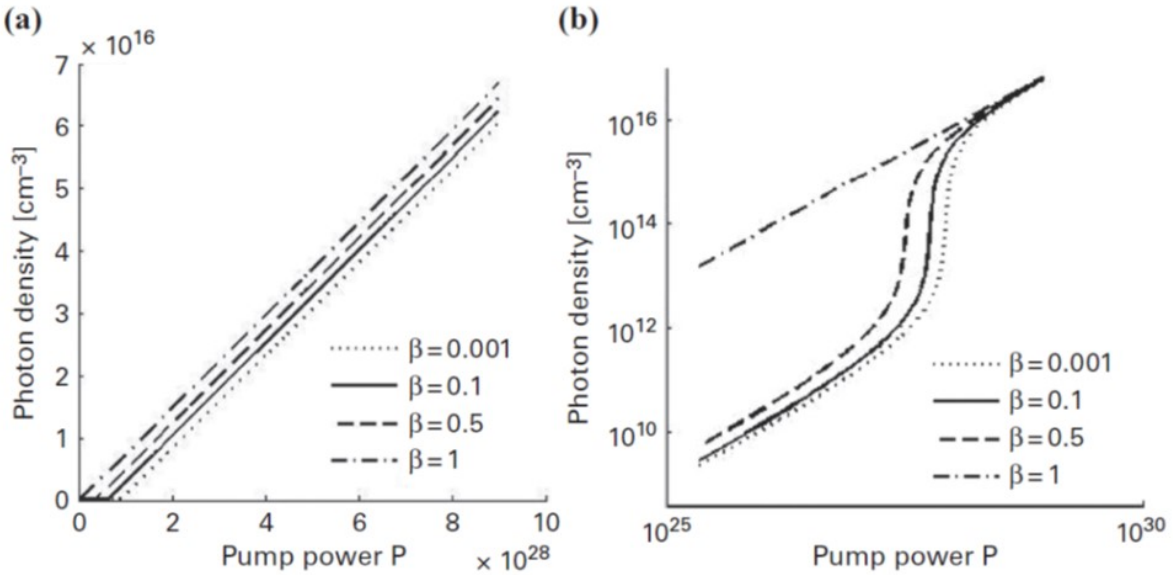

Figure 4.2: Simulated light-light curve pump power (output) vs photon density (input) in nanolaser for different values of spontaneous emission factor β, plotted in (a) linear and (b) log scale. [3]

V_a/Γ_k, in which the mode-gain overlap factor Γ_k describes the spatial overlap between the mode and the active region. Thus, if the mode is poorly confined, $\Gamma_k \ll 1$, F_p will remain small despite the small active region.

Since F_p is positively related to the modulation speed of a device, it is an important figure of merit in high-speed lasers design. However, we note that the Purcell factor F_p is the sum of contributions $F_{p,mnp}$ from each cavity mode present. Obviously, a higher emission into the lasing mode is desirable, as it allows a more efficient use of carriers, given that the emission into other modes is wasteful. From this point of view, therefore, the actual essential figure of merit is not the Purcell factor $F_{p,mnp}$, but the spontaneous emission factor β:

$$\beta = \frac{P_{P,\text{lasing}}}{\sum_{mnp} P_{P,\text{map}} + \zeta} \leq \frac{P_{P,\text{lasing}}}{\sum_{\text{mnp}} P_{P,\text{mnp}}} = \frac{F_{\text{P,lasing}}}{\sum_{\text{mnp}} F_{P,\text{mnp}}}, \tag{4.8}$$

here, the summation is over all the cavity modes, and ζ is the probability of spontaneous emission into free space. The value of β is brought closer to its theoretical limit $\beta = 1$ when one summation term is increased and other terms are suppressed, for example, when the unwanted cavity modes are eliminated, and ζ is minimized.

In the steady state, the photon density S is:

$$S = \frac{\Gamma_E \beta(n) R_{sp}(n)}{1/\tau_p - \Gamma_E R_{st}(n)}.$$

The influence of β (and F_p) on the light-light curve and the threshold condition is illustrated in Fig. 4.2, which shows the light-light curve for different values of β. On light-light curves plotted in linear scale (Fig. 4.2(a)), the "kink" is practically invisible for the curve with a different β (e.g., β of 0.001 and 0.1). Nanolaser light-light curves are usually plotted in log scale, as shown in Fig. 4.2(b), to demonstrate the subthreshold behavior more clearly. This kink is often referred to as the lasing threshold. However, as β becomes larger, the kink is gradually replaced by an increasingly smoother feature and eventually completely disappears in the extreme case of $\beta = 1$. While β is typically of the order of $1 \cdot 10^{-5}$ for conventional semiconductor lasers, the range of values used in Fig. 4.2 is typical for nanolasers.

Questions

1. Name the main types of micro- and nanolasers.
2. What is the difference between edge emitting laser and vertical cavity surface emitting laser?
3. What is the spontaneous emission factor and how does it influence the light-light curve?

References

1. Ning C. Z. Semiconductor nanolasers and the size-energy-efficiency challenge: a review //Advanced Photonics. – 2019. – V. 1. – №. 1. – P. 014002.
2. Zhang Y. et al. Photonic crystal disk lasers //Optics letters. – 2011. – V. 36. – №. 14. – . 2704-2706.
3. Gu Q., Fainman Y. Semiconductor nanolasers. – Cambridge University Press, 2017.

Chapter 5

Laser-matter interaction: Light absorption

5.1 Optics of metals and semiconductors

Over a wide frequency range, the optical properties of metals can be explained by a Drude-Lorentz model, where a gas of free electrons with the density n is moving against a fixed background of positive ion cores. For alkali metals, the range extends up to the ultraviolet, while for most noble metals interband transitions occur at visible frequencies, limiting the validity of this approach. In the plasma model, the details of the lattice potential and electron-electron interactions are not taken into account. Instead, it is simply assumed that some aspects of the band structure are incorporated into the effective optical mass m of each electron. The electrons oscillate in response to the applied electromagnetic field, and their motion is damped via collisions occurring with a characteristic collision frequency $\gamma = 1/\tau$. τ is known as the relaxation time of the free electron gas.

One can write a simple equation of motion for an electron of the plasma sea subjected to an harmonic external electric field $\mathbf{E}$:

$$m\ddot{\mathbf{x}} + \gamma\dot{\mathbf{x}} = -e\mathbf{E}_0 e^{-i\omega t}. \tag{5.1}$$

Solving this equation with the connection with macroscopic polarization taken into account, will determine dielectric function as:

$$\epsilon'(\omega) = 1 - \frac{\omega_p^2}{\omega^2 + \gamma^2}, \tag{5.2}$$

$$\epsilon''(\omega) = \frac{\omega_p^2 \gamma}{\omega(\omega^2 + \gamma^2}, \tag{5.3}$$

where $\omega_p^2 = \frac{ne^2}{\epsilon_0 m}$ is the plasma frequency of the free electron gas.

Whereas our description up to this point has assumed an ideal free-electron metal, we will now compare the model with an example of a real metal. In the free-electron model, $\epsilon \to 1$ at $\omega >> \omega_p$. For noble metals (e.g. Au, Ag, Cu), an extension to this model is needed in the region $\omega > \omega_p$ (where the response is dominated by free s electrons), since the filled d band close to the Fermi surface causes a highly polarized environment. This residual polarization due to the positive background of the ion cores can be described by adding an extra-term, and the dielectric function can be written as:

$$\epsilon(\omega) = \epsilon_\infty - \frac{\omega_p^2}{\omega^2 + i\gamma\omega}, \tag{5.4}$$

where ϵ_∞ corresponds to the localized electron polarization.

The validity limits of the free-electron description 5.1 are illustrated for the case of gold in Fig.5.1. It shows the real and imaginary components ϵ' and ϵ'' for a dielectric function, fitted to the experimentally determined dielectric function of gold [Johnson and Christy, 1972]. Clearly, at visible frequencies the applicability of the free-electron model fails down due to the occurrence of interband transitions, leading to an increase in ϵ''.

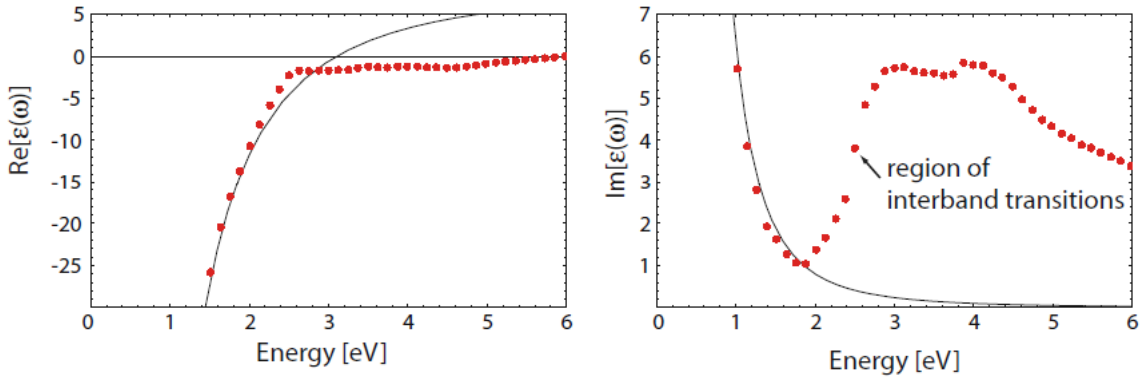

Figure 5.1: Dielectric function $\epsilon(\omega)$ of the free electron gas (solid line) fitted to the values in the reference of the dielectric data for gold (dots) [1]. Interband transitions limit the validity of this model at visible and higher frequencies.

5.2 Carriers dynamics

Under the action of laser pulsed radiation with an energy density Q, a pulse duration τ_p and photon energy $\hbar\omega$ on a semiconductor surface nonequilibrium carriers are generated due to interband absorption. The equation for nonequilibrium carrier density can be written as:

$$\frac{\partial n_c}{\partial t} = D\frac{\partial^2 n_c}{\partial z^2} + G - R, \tag{5.5}$$

where D is the diffusion coefficient, G and R are the generation and the recombination rates, respectively.

Since the absorption of a single photon from a laser beam is accompanied by the production of one electron-hole pair, the rate of the generation of free carriers can be determined by the rate of the absorption of energy in the near-surface layer divided by the photon energy $\hbar\omega$:

$$G(t,z,T) = \frac{\alpha(t,z,T)(1-R_c)}{\hbar\omega\tau_p} Q exp(-\int_0^Z \alpha(t,z',T)dz') \approx G_0 exp(-\alpha z), \tag{5.6}$$

where $\alpha = \alpha^L + \alpha^{NL}$ is the sum of linear and nonlinear coefficients, T is the temperature and R_c is the optical reflection coefficient.

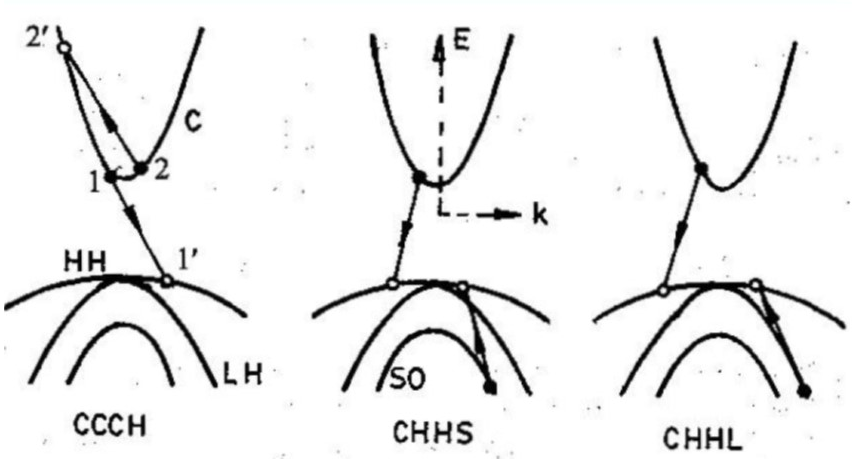

Figure 5.2: $E-k$ diagrams for various Auger recombination processes in a direct band gap semiconductor.

Auger recombination is a fundamental process of semiconductor material. It is a band-to-band three-particle scattering process that involves either: i) an e-e collision in the conduction band and a recombination with a hole in the valence band or ii) a h-h collision in the valence band followed by a recombination with an electron in the conduction band. Three distinct paths are shown in Fig. 5.2: CCCH, CHHS, CHHL, where letter C stands for conduction electron, H for heavy-hole, L for light-hole and S for a split-off hole. In CCCH, two electrons in the conduction band and one hole in the heavy hole band are involved. In CHHS, one electron in the conduction band, one hole in the heavy hole band, and one hole in the split-off band interact. In CHHL, one electron from the conduction band and two holes in the heavy hole band scatter.

A collision occurs between two carriers in the same band (e-e or h-h): the energy from the recombining carrier is transferred to the remaining carrier. Note that both the energy and the momentum must be conserved to complete the scattering event. The excited or hot carrier will quickly thermalize with the lattice via phonon emission and generate

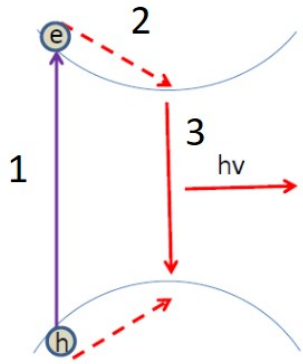

Figure 5.3: E-k diagram of radiative recombination. 1 – absorption: e-h pair generation, 2 – intraband relaxation: e(h)-phonon scattering and 3 – interband relaxation: e-h annihilation and photon emission.

heat. The Auger recombination process in semiconductors can either be direct or phonon-assisted. The CCCH and CHHS are believed to be the two dominant processes. The net rate of Auger recombination in steady-state can be written as:

$$R_A = C_e \left(n^2 p - n_0^2 p_0\right) + C_p \left(n p^2 - n_0 p_0^2\right), \tag{5.7}$$

where C_e and C_p denote the non-radiative Auger recombination coefficients for electrons and holes, respectively. These coefficients are independent of the carrier density. Using the assumptions $n = p = n_c$ the non-radiative Auger recombination rate can be written as:

$$R_A = (C_e + C_p) = C n_c^3, \tag{5.8}$$

where C is the aggregate Auger non-radiative coefficient.

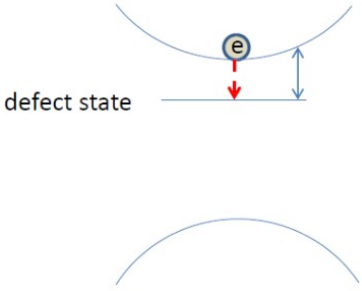

Figure 5.4: Scheme of non-radiative recombination process

A radiative recombination occurs in indirect band semiconductors. Some details of this recombination are shown in Fig. 5.3. After the absorption of the photon an electron-hole pair is generated. Hot carriers give off heat to phonons and after annihilation of the

electron with the hole a photon radiates. The radiative recombination rate is proportional to the concentration of both types of carriers. The radiative recombination rate using the previous assumptions can be written as:

$$R_r = Bn_c^2, \tag{5.9}$$

where the constant coefficient B is obtained from a spectral integration of the spontaneous emission rate.

The third recombination process is the non-radiative trap recombination. A scheme of this recombination mechanism is given in Fig. 5.4. In general, the rate of this process corresponds to the electron and trap concentrations. In the simplest case, the non-radiative rate can be written as:

$$R_{nr} = An_c, \tag{5.10}$$

where A is the constant of the non-radiative recombination depending on the trap cross-section.

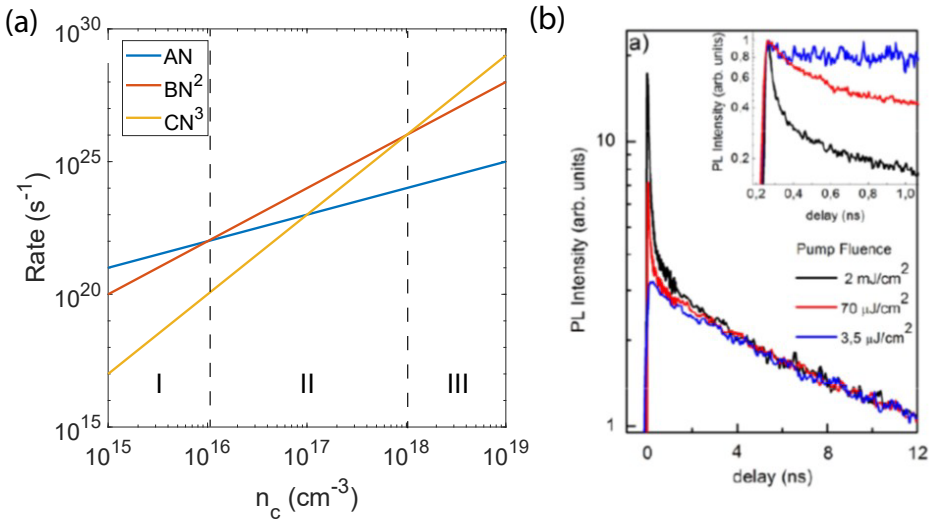

Figure 5.5: (a) Recombination rates: I - nonradiative, II - radiative and III - Auger. (b) Time-resolved measurements for various fluences [6].

Taking into account the three recombination processes above, the extremely short duration of laser pulse, and neglecting the diffusion, Eq. 5.5 can be rewritten as:

$$\frac{\partial n_c}{\partial t} = -An_c - Bn_c^2 - Cn_c^3. \tag{5.11}$$

Solving this equation by taking into account all recombination processes is complicated. However, a variation of power can make distinguishably different contributions of various processes. Fig. 5.5(a) presents the dependence of the rates on the carrier density. There

are three different regions with a pronounced domination of different processes: I - nonradiative, II - radiative and III - Auger.

The dominance of different recombination processes depending on the carrier concentration is clearly seen in the time-resolved photoluminescence measurements. The carrier control is available by varying the excitation power. Fig. 5.5(b) demonstrates the changes of photoluminescence lifetimes depending on the pump intensity.

5.3 Principles of Electromagnetic heating

Temperature distributions induced by the absorption of laser radiation have been calculated based on the heat equation. In the most general case, the temperature $T = T(x,t) = T(x_\alpha, t)$ is a function of both the spatial coordinates x_α and the time t. With fixed laser parameters the temperature distribution depends on the optical absorption within the irradiated zone and on the transport of heat out of that zone. In the absence of heat transport by convection or thermal radiation, the heat equation can be written as:

$$\rho(T)c_{\mathrm{p}}(T)\frac{\partial T(x,t)}{\partial t} - \nabla[\kappa(T)\nabla T(x,t)] = Q(x,t), \tag{5.12}$$

where ρ is the mass density, $c_p(T)$ is the specific heat at a constant pressure, κ is the thermal conductivity and $Q(x,t)$ is the heat source.

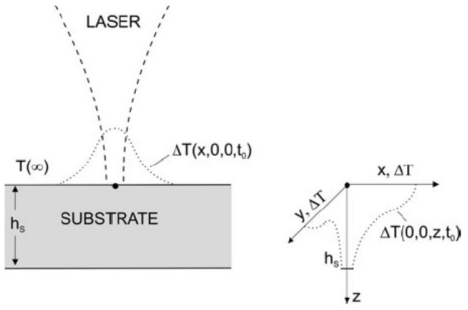

Figure 5.6: Infinite slab of uniform thickness h_s irradiated by perpendicular laser beam. The laser-induced temperature increase on the surface $z = 0$ and along the z-direction is shown (dotted curves). The temperature far away from the irradiated area is $T(\infty)$.

For a laser beam focused in the spot the general solution for temperature distribution in Eq. 5.12 is $T(r) \sim \exp(-r^2/L_{\mathrm{tot}}^2)$, where L_{tot} is the characteristic width of temperature distribution. This width is determined by the diffusion length ($\sim (\tau_{pulse} D)^{(1/2)}$) and the depth of penetration of electromagnetic radiation ($\sim \lambda/Im(n)$). It is perfectly clear that for dielectric diffusion length is small because dielectrics have low conductivity and a large penetration depth because the imaginary part of the refractive index is low. Metals show the opposite: their conductivity and imaginary refractive index are high.

5.4 Principles of ultrafast electromagnetic heating

In metals, light is almost exclusively absorbed by free-electron transitions within the conduction band. In the electron system, the excitation energy is thermalized within, typically, 10 fs to 1 ps. Thermalization between the electron subsystem and the lattice is much slower, typically of the order of 1–100 ps, depending on the strength of electron-phonon coupling Γ_{e-ph}. Thus, femtosecond laser excitation generates a hot electron gas. The transient non-equilibrium between the hot electrons and the lattice can be described by temperatures T_e and T, which can be calculated from the corresponding heat equations. This description is referred to as a two-temperature model. In the laboratory system, the (coupled) nonlinear equations for T_e and T can be written, in a more general form, as:

$$C_{\mathrm{e}}\left(T_{\mathrm{c}}\right)\frac{\partial T_{\mathrm{e}}}{\partial t}=\nabla\left[\kappa_{\mathrm{e}}\left(T_{\mathrm{e}},T\right)\nabla T_{\mathrm{e}}\right]-\Gamma_{\mathrm{e-ph}}\left(T_{\mathrm{e}}\right)\left[T_{\mathrm{e}}-T\right]+Q\left(x_{\alpha},t\right), \tag{5.13}$$

and

$$C(T)\frac{\partial T}{\partial t}=\nabla[\kappa(T)\nabla T]+\Gamma_{\mathrm{e-ph}}\left(T_{\mathrm{e}}\right)\left[T_{\mathrm{e}}-T\right], \tag{5.14}$$

where C_e and C are the heat capacities (per unit volume) of the electron and the lattice subsystems, respectively.

The two-temperature model describes the laser excitation of conduction band electrons and the subsequent energy transfer from the hot electrons to the lattice vibrations via electron-phonon coupling. The model assumes the validity of the heat equation for ultrashort laser pulses. In other words, it assumes that the energy distribution of electrons is thermalized and can be described by a temperature T_e. In many applications of the abovementioned formulas, the coefficients have been assumed as constant. This is, however, inadequate in most cases. The consideration of the influence of the electron temperature T_e on the electron-phonon coupling and the electron heat capacity is quite important.

Fig. 5.7 shows the temporal dependence of the electron and the lattice temperatures calculated from the two-temperature model for 100 nm thick films of Au and Ni. These metals are representative examples for weak and strong electron-phonon coupling (EPH) ($\Gamma_{e-ph}(Au) \approx 2.3 \cdot 10^{10} W/cm^3K; \Gamma_{e-ph}(Ni) \approx 3.6 \cdot 10^{11} W/cm^3K$). The differences in EPH are directly revealed in the different behaviour of temperatures T_e and T . In particular, the time required to reach thermal equilibrium in Au is almost ten times longer than for Ni. Another consequence is the temperature gradient that builds up between the front and the rear sides. In Au, Γ_{e-ph} is small and thus $l_e \approx (D_e C_e/\Gamma_{e-ph})$ large. Therefore, the absorbed energy can spread into deeper parts of the sample and thereby diminish the energy density in the surface region. Films with a thickness comparable to l_e, are heated almost homogeneously. The opposite behaviour is found for Ni. Strong electron-phonon coupling causes a rapid cooling of hot electrons and thereby prevents long-range energy transport by electron diffusion.

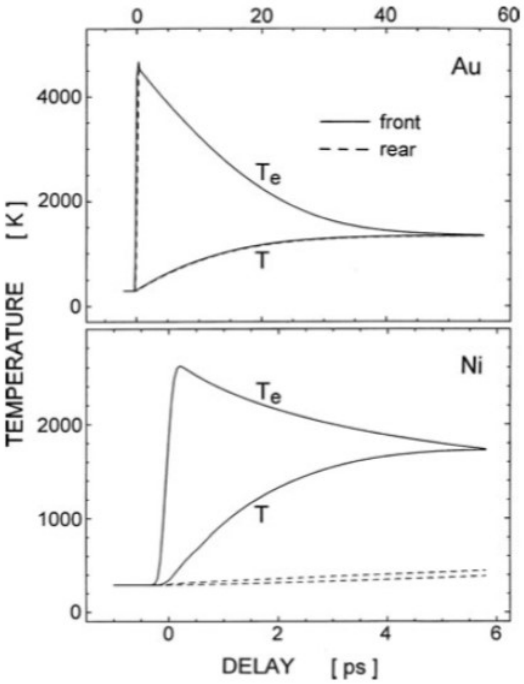

Figure 5.7: Temporal dependence of the electron temperature T_e and the lattice temperature T calculated for 100 nm films of Au and Ni irradiated with 200 fs pulses. Solid curves show the temperature at the surface (front side) of films; dashed curves show the temperature at the rear side. With Ni, thermal equilibrium is reached about 10 times faster than with Au

The two-temperature model permits a qualitative and, in certain cases, even a semi-quantitative interpretation of ultrashort-pulse laser-metal interactions. For example, Fig. 5.7 explains the differences in damage (melting) thresholds for noble metals and transition metals, and thereby the importance of electron-phonon coupling. Due to rapid energy transport by hot electrons, the damage threshold observed (experimentally) with Au is higher than for Ni. This agreement also proves the thermal character of laser-metal interactions for fs-laser pulses. It should be noted, however, that with ns-pulses the damage threshold is higher for Ni compared to Au.

5.5 Ultrafast Optical Techniques

With the development of ultrashort-pulse lasers, fast optical techniques for investigating transient laser-induced phenomena have become of increasing importance. Clearly, the classification between 'quasistationary' diagnostic techniques and 'ultrafast' optical techniques is somewhat arbitrary. Transient laser-induced phenomena are used in temporal evolutions

of surface reflectivities, surface deformations, melting, ablation thresholds and other characteristic. A schematic picture of an experimental setup for time-resolved microscopy is presented on the Fig. 5.8.

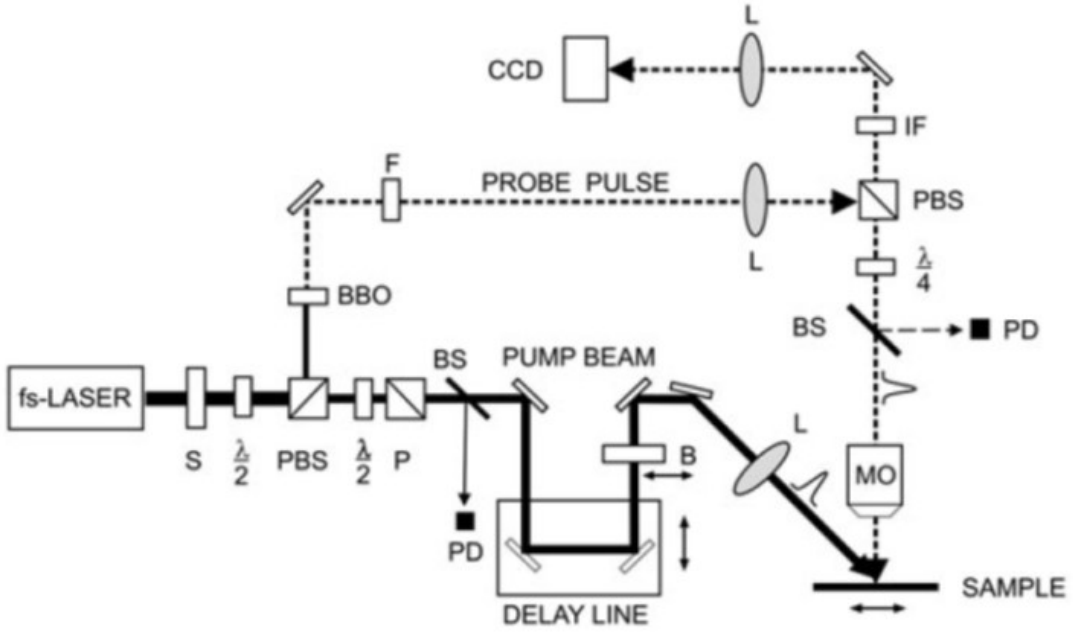

Figure 5.8: An experimental setup was employed for fs-time-resolved microscopy. Part of the fs-laser beam is used as a probe beam which is frequency-doubled (BBO crystal). The signal reflected from the sample surface is imaged onto a CCD camera. S: electromechanical shutter; PBS: polarizing beam splitter; P: polarizer; BS: beam splitter; L: lens; F: bandpass filter; PD: photodiode; MO: microscope objective; IF: interference filter.

Questions

1. What are the main recombination processes and how do they depend on the charge carrier concentration?
2. How does the recombination rate of charge carriers depend on the power of the exciting radiation?
3. What is the two-temperature model?

References

1. Johnson P. B., Christy R. W. Optical constants of the noble metals //Physical review B. – 1972. – V. 6. – №. 12. – P. 4370.

2. Maier S. A. Plasmonics: fundamentals and applications. - Springer Science & Business Media, 2007.

3. Koroteev N. I., Shumai I. L. Physics of intense laser radiation. - 1991.

4. Bäuerle D. Laser processing and chemistry. - Springer Science & Business Media, 2013.

5. Chuang S. L. Physics of optoelectronic devices. - 1995.

6. Karpov S. ABC-model for interpretation of internal quantum efficiency and its droop in III-nitride LEDs: a review //Optical and Quantum Electronics. - 2015. - V. 47. - № 6. - P. 1293-1303.

Chapter 6

Optical Heating in Nanophotonics

6.1 Optical Heating Equations

For solving the problem of optical heating let us start with a general equation for the heat problem:

$$\rho c_p \partial T/\partial t = \nabla(\kappa \nabla T) + (\partial Q/\partial t), \tag{6.1}$$

where ρ is the material density, c_p is the heat capacity, κ is the thermal conductivity, T is the temperature and Q is the amount of heat received per unit volume of material.

In this particular solution the temperature dependence of ρ, c_p, κ and $(\partial Q/\partial t)$ is negligible in most cases. When describing heating, Eq.6.1 can be rewritten as:

$$\partial T/\partial t = \chi \Delta T + (\rho c_p)^{-1} (\partial Q/\partial t), \tag{6.2}$$

where $\chi = \kappa/\rho c_p$ is the thermal diffusivity.

A laser beam propagates along the axis Z and falls on the XY plane of material and creates a volume heat source:

$$\partial Q/\partial t = \alpha I(r,t), \tag{6.3}$$

where α is the absorption coefficient and $I(r,t)$ is the distribution of light intensity (in the region $z > 0$). In the simplest case of Gaussian beam, the following expression is obtained:

$$I(r,t) = (1-R) I_0 \exp(-\alpha z) \exp\left[-\left(x^2+y^2\right)/a^2\right] f\left(t/\tau_p\right), \tag{6.4}$$

where I_0 is the intensity of radiation incident on the absorbing medium from the outside, R is the optical reflection coefficient and a is the radius of Gaussian beam. Function $f\left(t/\tau_p\right)$ describes the temporal shape of the laser pulse with the duration τ_p.

Since the Eq. 6.2 is linear, it is also valid for the increase of body temperature $T' = T - T_0$, where T_0 is body temperature in the absence of optical excitation. We will consider

the process of heating a material in the absence of heat exchange with the environment using the following boundary condition:

$$-\left. q_z \right|_{z=0} = \chi \left. \frac{\partial T'}{\partial z} \right|_{z=0} = 0. \tag{6.5}$$

The method of green functions is convenient for solving the Eq. 6.2. Indeed, let us assume $G\left(r-r', t-t'\right)$ is the solving for heat source localised in $r=0$ and has instant impulse, that is, for which it is true:

$$\frac{1}{\rho c_p}\left(\frac{\partial Q}{\partial t}\right) \rightarrow A\delta\left(\boldsymbol{r}-\boldsymbol{r}'\right)\delta\left(t-t'\right). \tag{6.6}$$

When Eq. 6.2 and the boundary conditions Eq. 6.5 are linear, solving the heat problem with an arbitrary source has the form:

$$T(r,t) = \frac{1}{\rho c_p}\int_{-\infty}^{t} dt' f\left[\frac{\partial Q}{\partial t}\left(r', t'\right)\right] G(r-r, t-t) d^3 r'. \tag{6.7}$$

For a point source Eq. 6.2 can be rewritten as:

$$\partial T'/\partial t = \chi \Delta . T' + A\delta(r)\delta(t) \tag{6.8}$$

Solving this equation taking into account the boundary conditions gives the following expression:

$$T'(r,t) = \frac{A}{(4\pi\chi t)^{3/2}} \exp\left(-\frac{r^2}{4\chi t}\right). \tag{6.9}$$

According to this expression, after an instant point energy increase the temperature in heat point has the temporal law of $T' \sim t^{-3/2}$, and the characteristic size of the heating area increases as $r_0 \sim (\chi t)^{1/2}$. According to all the above, the general solutions for continuous-wave laser excitation can be written as:

$$\begin{gathered}\frac{\partial T}{\partial t} = \frac{\alpha(1-R)I_0}{2\rho_0 c_p}\frac{1}{1+4\chi t/a^2}\exp\left(-\frac{x^2+y^2}{a^2+4\chi t}\right)\exp\left(\alpha^2\chi t\right)\left\{\exp(\alpha z)\operatorname{erfc}\left[\alpha(\chi t)^{1/2}+\frac{z}{(4\chi t)^{1/2}}\right]+\right. \\ \left.+\exp(-\alpha z)\operatorname{erfc}\left[\alpha(\chi t)^{1/2}-\frac{z}{(4\chi t)^{1/2}}\right]\right\}\theta(t)\end{gathered}, \tag{6.10}$$

where $\theta(t)$ is Heaviside function and $\operatorname{erfc}(x) = \frac{2}{\sqrt{\pi}}\int_x^\infty e^{-t^2}\mathrm{d}t$ is the complementary error function.

The maximum rate of temperature increase is observed on the surface of the irradiated substance (z=0) along the axis of the laser beam (x=y=0):

$$\frac{\partial T'}{\partial t}(r=0,t) = \frac{\alpha(1-R)I_0}{\rho_0 c_p}\frac{\exp\left(\alpha^2\chi t\right)\operatorname{erfc}\left[\alpha(\chi t)^{1/2}\right]}{1+4\chi t/a^2} \tag{6.11}$$

According to Eq. 6.11 at the initial stage ($t \leqslant \min\{a^2/\chi, 1/\alpha^2\chi\}$) thermal conductivity does not affect the heating rate which is constant ($\partial T/\partial t = \alpha(1-R)I_0/\rho_0 c_p$). The physical meaning of the value a^2/χ is the characteristic time during which the influence of the heat source extends to the distance of the transverse size of the laser beam a.

Similarly, it can be stated that the finiteness of the penetration depth of light in the matter ($d = \alpha^{-1}$ absorption length) will manifest itself in heating only after the characteristic time $d^2/\chi = 1/\alpha^2\chi$. Thus, at times $t \leqslant \min\{a^2/\chi, 1/\alpha^2\chi\}$ the maximum temperature of a substance increases over time according to a linear law: $T \sim t$.

Let us assume that the transverse size of the laser beam is significantly greater than the absorption length ($a \gg d$). Then, as time increases, the heat transfer into the medium "switch on" firstly, which results in a decrease in the rate of heating. For condition $1/\alpha^2\chi \leqslant t \leqslant a^2/\chi$ Eq. 11 takes the form:

$$\frac{\partial T'}{\partial t} \approx \frac{(1-R)I_0}{\rho_0 c_p}\frac{1}{(\pi\chi t)^{1/2}} \sim t^{-1/2}. \tag{6.12}$$

Therefore, the temperature increment grows sublinearly ($T \sim t^{1/2}$). Time $t \geq a^2/\chi$ after the laser exposure, thermal conductivity in the direction along the surface begins to influence the temperature increase. The heating rate rapidly decreases. At the condition ta^2/χ, the solution is:

$$\left.\frac{\partial T'}{\partial t}\right|_{t\to\infty} \approx \frac{(1-R)I_0\pi a^2}{\rho_0 c_p(4\pi\chi t)^{3/2}}. \tag{6.13}$$

Maximum temperature T'_{max} at ta^2/χ is conditioned by the law:

$$T' = T'_{\max} - \frac{(1-R)I_0\pi a^2}{2\rho_0 c_p \pi\chi(4\pi\chi t)^{1/2}}. \tag{6.14}$$

The maximum temperature T'_{max} is defined as the integral Eq. 6.11: $T'_{max} = T'(r = 0, t = \infty$. In case $\alpha a \gg 1$ it can be estimated as:

$$T'_{\max} \sim \frac{(1-R)I_0 a}{\rho_0 c_p \chi} = \frac{(1-R)\mathfrak{P}}{\kappa a}, \tag{6.15}$$

where $\mathfrak{P} = a^2 I_0$ is the total power of a Gaussian beam with the radius a and the intensity I_0.

6.2 Nanoparticle Heating

The power absorbed by a nanoparticle (NP) can be simply expressed using the absorption cross-section σ_{abs} :

$$Q = \sigma_{\text{abs}} I \tag{6.16}$$

where I is the intensity of the incoming light. In the case of a plane wave $I = n_s c_0 \varepsilon_0 |\mathbf{E}_0|^2 / 2$.

Heat generation can also be derived from the heat power density $q(\mathbf{r})$ inside the NP such that $Q = \int_V q(\mathbf{r}) \mathrm{d}^3 r$, where the integral runs over the NP volume V. Since the heat originates from Joule effects, the heat power density reads:

$$q(\mathbf{r}) = \frac{1}{2} \mathrm{Re} \left[\mathbf{J}^\star(\mathbf{r}) \cdot \mathbf{E}(\mathbf{r}) \right], \tag{6.17}$$

where $\mathbf{J}(\mathbf{r})$ is the complex amplitude of the electronic current density inside the NP. As $\mathbf{J}(\mathbf{r}) = i\omega\mathbf{P}$ and $\mathbf{P} = \varepsilon_0 \varepsilon(\omega)\mathbf{E}$ this ends up with

$$q(\mathbf{r}) = \frac{\omega}{2} \mathrm{Im}(\varepsilon(\omega)) \varepsilon_0 |\mathbf{E}(\mathbf{r})|^2. \tag{6.18}$$

Heat generation is thus directly proportional to the square of the electric field inside the NP. In practice, this results in the two ways of calculating the heat power Q absorbed by a given NP. For geometries where the absorption cross-section is known (for example for spherical NPs), Q can be estimated using Eq. 6.16. However, for more complicated morphologies for which there is no simple analytical expression available, the computation of the inner electric field amplitude $\mathbf{E}(\mathbf{r})$ is required to calculate $q(\mathbf{r})$ from Eq. 6.18.

While the computation of the delivered heat power Q turns out to be a purely optical problem as explained in the previous section, the determination of the steady-state temperature distribution $T(\mathbf{r})$ inside and outside the NP is based on the solution of the heat diffusion equation:

$$\begin{array}{ll} \nabla \cdot [\boldsymbol{\kappa}(\mathbf{r}) \nabla T(\mathbf{r})] = -q(\mathbf{r}) & \text{inside the NP,} \\ \nabla \cdot [\boldsymbol{\kappa}(\mathbf{r}) \nabla T(\mathbf{r})] = 0 & \text{outside the NP,} \end{array} \tag{6.19}$$

where $\boldsymbol{\kappa}(\mathbf{r})$ is the thermal conductivity. For a spherical NP of the radius R, simple calculations gives the temperature increase:

$$\begin{array}{ll} \delta T(r) = \delta T_{\mathrm{NP}} \frac{R}{r}, & r > R \\ \delta T(r) \approx \delta T_{\mathrm{NP}}, & r < R \end{array} \tag{6.20}$$

where δT_{NP} is the temperature increase of the NP. Remarkably, while the heat power density $q(\mathbf{r})$ can be very far from uniform within the NP, the temperature at equilibrium generally, on the contrary, perfectly uniform inside the NP. This is due to the much larger thermal conductivity of material compared to that of the surroundings (air, glass or other media). The actual temperature increase experienced by a NP depends on numerous parameters, namely, its absorption cross-section, its shape, the thermal conductivity of the surrounding medium, the wavelength and the irradiance of the incoming light. For a spherical NP, its temperature increase is related to the absorbed power $Q = \sigma_{\mathrm{abs}} I$ according to:

$$\delta T_{\mathrm{NP}} = \frac{Q}{4\pi \kappa_s R}, \tag{6.21}$$

where $\kappa(r)$ is the thermal conductivity of the surrounding medium.

This steady-state temperature profile is usually established very fast when working with NPs. The typical duration τ_{tr} of the transient regime depends on the characteristic size L of the system (for instance the radius R for a sphere) rather than on the temperature increase:

$$\tau_{\mathrm{tr}} \sim L^2 \frac{\rho c_{\mathrm{p}}}{3\kappa_{\mathrm{s}}}, \tag{6.22}$$

where ρ is the mass density of the NP and c_p is its specific heat capacity at constant pressure. For example, for spherical NPs with various diameters in water the values of τ_{tr} are shown on Fig.6.1.

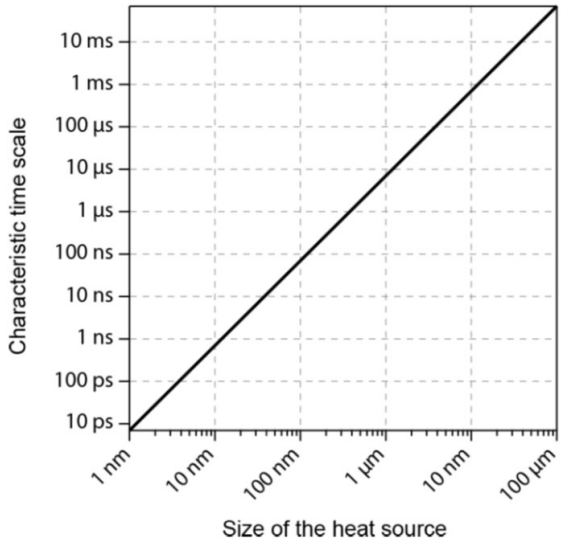

Figure 6.1: Characteristic time scale of heat diffusion in water as a function of the heat source size. [2]

The absorption of laser pulse energy by a NP can be described as a three-step process, each of these steps involving different time scales. During the interaction with the laser pulse, part of the incident pulse energy is absorbed by the gas of free electrons of the NP, much lighter and more reactive than the ion lattice. The electron gas thermalizes very fast, for gold the time scale is approximately τ_e=100 fs. This leads to a state of non-equilibrium within the NP: the electron temperature Te of the electron gas increases while the temperature of the lattice (phonons) T_p remains unchanged.

Subsequently, this hot electron gas relaxes (cools down), through internal electron-phonon interaction characterized by a time scale τ_{e-ph} to thermalize with the ions of the gold lattice. This time scale does not depend on the size of the NP except for the NPs smaller than 5 nm due to confinement effects. Above this size and for a moderate pulse energy, the time scale is constant and equals τ_{e-ph}= 1.7 ps for gold. At this point, the NP

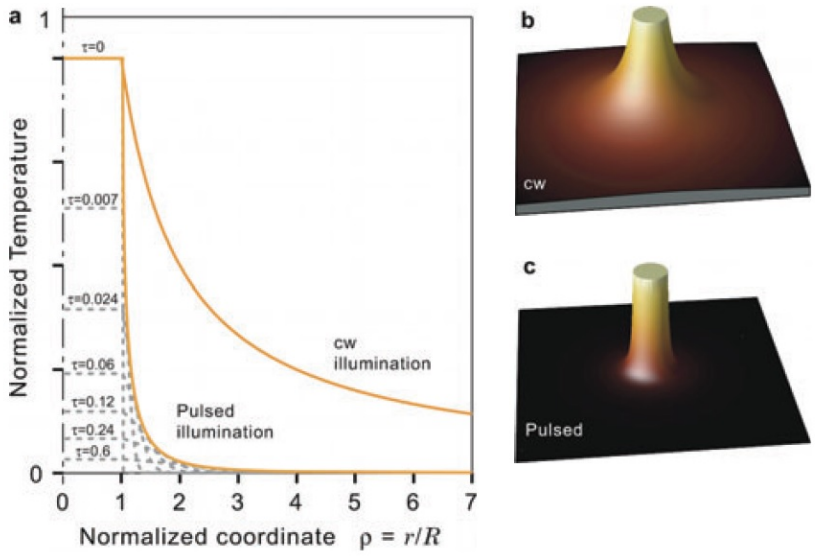

Figure 6.2: Figure comparing the spatial extension of the temperature profile in CW and pulsed illuminations. a) Radial profiles of temperature in both cases. In the case of pulsed illumination, temperature profiles at different normalized times $\tau = t/\tau_{tr}$ are represented (dashed lines) along with the associated temperature envelope. b) Three-dimensional representation of the temperature profile around a NP under CW illumination. c) Three-dimensional representation of the temperature envelope around a NP subsequent to a single femtosecond-pulse illumination [3]

is in internal equilibrium at a uniform temperature ($T_e = T_p$) but is not in equilibrium with the surrounding medium that is still at the initial ambient temperature.

The energy diffusion from the NP to the surroundings usually occurs at a longer characteristic time scale τ_{tr} (see Eq. 6.22) and leads to cooling the NP and heating the surrounding medium. During this process, the total absorbed energy reads as $\sigma_{\text{abs}}\langle I\rangle/f = \sigma_{\text{abs}}F$ where f is the pulsation rate and F is the fluence of the laser pulse. Different regimes can be observed depending on the pulse duration compared with τ_{tr}. When the pulse duration is short enough and/or the NP is small enough, the three steps can be considered to happen successively. In this regime, the initial temperature increase reaches its maximal value:

$$\delta T_{\text{max}} = \frac{\sigma_{\text{abs}}\langle I\rangle}{V\rho c_{\text{p}} f} = \frac{\sigma_{\text{abs}}F}{V\rho c_{\text{p}}}, \tag{6.23}$$

where V is the volume of the NP.

Thermodynamics is also influenced by the pulsation rate f of the laser. If f is too high, the particle may not have enough time to completely cool down between two successive pulses. This leads to a regime where the NP is permanently hot, as shown in Fig. 6.3. In practice, such a regime is achieved when $f > 1/\tau_{tr}$ discriminate between both regimes, a

dimensionless number ξ can be introduced, so that $\xi = f\tau_{tr}$. For $\xi \ll 1$, temperature confinement can be expected and is subject to the following law:

$$T(r,t) = \frac{\sigma_{abs}F}{c_{\mathrm{ps}}\rho_{\mathrm{s}}} \frac{1}{(4\pi D_{\mathrm{s}}t)^{3/2}} \exp\left(-\frac{r^2}{4D_{\mathrm{s}}t}\right). \tag{6.24}$$

Otherwise, extended temperature dependence like Eq. 6.20 is dominant. A comparison of these two regimes is presented in Fig. 6.2, where temporal evolution of temperature is also shown.

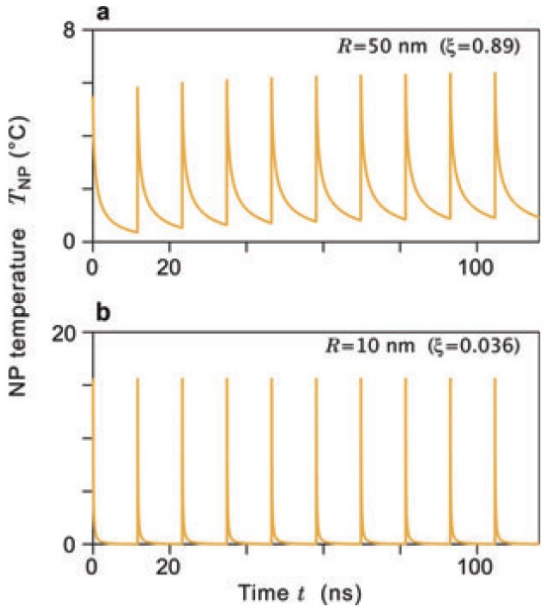

Figure 6.3: Temporal evolution of the temperature of a spherical gold NP with the radius R illuminated by a train of pulses with the repetition rate f =86MHz and the average irradiance $I = 1mW/m^2$: a) R=50 nm; b) R=10 nm. [3]

6.3 Optimal Conditions for NPs Optical Heating

In order to provide a deep understanding of the origin of strong heating of low-loss dielectrics, we consider the case of resonant heating, when an external wave is coupled with an eigenmode of the nanoparticle. The general expression for the absorbed electromagnetic power Q is:

$$Q = \frac{1}{2}\,\mathrm{Re}\int_V \mathbf{J}^{\star}(\mathbf{r})\cdot\mathbf{E}(\mathbf{r})\mathrm{d}^3r \tag{6.25}$$

where $\mathbf{J}(\mathbf{r})$ is the current density, $\mathbf{E}(\mathbf{r})$ is the electric field inside the material, and the integration is taken over the volume of the nanoobject V. From this formula, it follows

that the stronger the electric field inside the material, the higher the absorbed power. The heating itself is caused by the Ohmic losses determined by the electric conductivity σ, yielding $J = \sigma E$. The imaginary part of the permittivity determines conductivity as $\sigma = \epsilon_0 \omega Im(\epsilon)$, where ϵ_0 and ω are the dielectric permittivity of vacuum and the incident light frequency, respectively.

Integration in Eq. 6.25 over an arbitrary nanoparticle volume supporting eigenmodes allows rewriting Eq. 6.25 in terms of the effective mode volume V_{eff} and the spatially averaged field enhancement factor $F = \langle |E|^2 \rangle / |E_0|^2$, which determines how much energy can be accumulated inside the nanoparticle and where $|E_0|$ is the incident electric field magnitude. Thus, we can rewrite Eq. 6.25 for the absorbed power as:

$$P \sim \sigma F^2 V_{\text{eff}}. \tag{6.26}$$

From Eq. 6.26, it is clear that the increasing Ohmic losses do not necessarily lead to a rise of light absorption by the nanoparticle. On the one hand, the imaginary part of the permittivity increases the conductivity but on the other hand, it suppresses the quality factor Q of the optical resonance; therefore, the factor σF^2 has to be considered in more detail.

The field enhancement factor near the nanoparticle resonance ω_0 can be expressed as $F \sim 1/(\omega_0^2 - \omega^2 - i\omega\gamma)$, where γ defines the total optical losses. The optical losses include both radiative and nonradiative (or Ohmic) losses $\gamma = \gamma_{rad} + \gamma_{Ohmic}$. The latter are proportional to $Im(\epsilon)$, hence the factor σF^2 at the resonant frequency ω_0 is proportional to $\sigma F^2 \sim \gamma_{Ohmic}/(\gamma_{rad} + \gamma_{Ohmic})^2$, from which it is clear that for high Ohmic losses the absorbed power tends to zero. Thus, at fixed γ_{rad} the maximal value of this factor $(\sigma F^2)_{\max} \sim 1/(4\gamma_{\text{rad}})$ can be achieved when $\gamma_{rad} = \gamma_{Ohmic}$. Radiative losses can be suppressed by assuming the resonant nanoparticle is much smaller than the wavelength λ, which is the case of small plasmonic nanoparticles, where $\gamma_{\text{rad}} \ll \gamma_{\text{Ohmic}}$. At the surface plasmon resonance $\omega = \omega_0$, the radiative losses are equal to $\gamma_{\text{rad}} \approx \omega_0^3/\omega_{\text{p}}^2(\pi D/\lambda)^3$, where ω_p is the plasma frequency. This estimation formula gives small values for γ_{rad} compared to ω_0 due to the ratio $(D/\lambda)^3$. As shown in Fig. 6.4(a), for small nanoparticles the resonance occurs only in the region of negative $Re(\epsilon)$, and maximal temperature is achieved at relatively small values of $Im(\epsilon)$, where $\gamma_{rad} = \gamma_{Ohmic}$. On the other hand, for bigger nanoparticles, which is the case of dielectric ones, the radiative losses for low order dipole modes are high and maximal heating is achieved at higher Ohmic losses (see Fig.6.4(b,c)). However, for higher order resonances, for example, quadrupole, one can expect small radiative losses and, thus, the maximal optimal heating for lower Ohmic losses, which is shown for higher $Re(\epsilon)$ in Fig. 6.4b,c.

Another factor, which is important for the absorption of light, is the effective mode volume inside the nanoparticle V_{eff}. Generally, the larger the volume of an arbitrary nanoparticle, the stronger the heating. However, the effective mode volume can significantly affect this dependence. For plasmonic nanoparticles ($Re(\epsilon) < 0$), the effective volume is defined by the skin depth, which is less than $\delta \approx 20$ nm for most metals in the visible range. Thus, the effective mode volume of plasmonic nanoparticles is $V_{eff} \approx \pi D^2 \delta$. Unlike

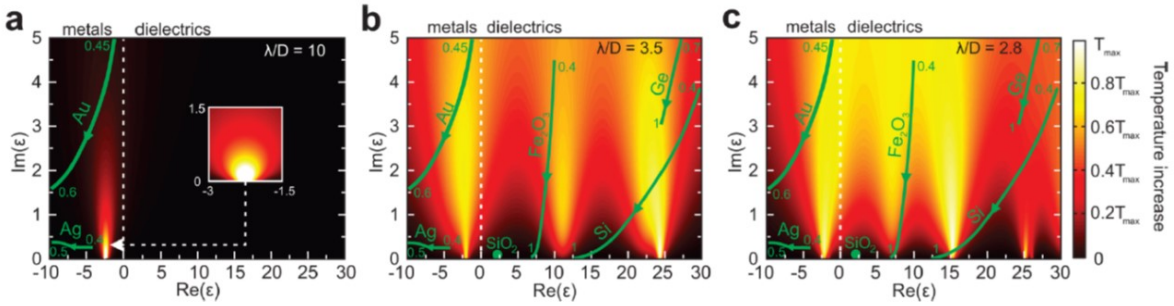

Figure 6.4: Resonant heating of a spherical nanoparticle. Theoretically calculated (Mie theory) heating maps for spherical nanoparticles with fixed wavelength (λ)/diameter (D) ratios for different real and imaginary parts of permittivity in a homogeneous medium (air): (a) $\lambda/D = 10$; (b) $\lambda/D = 3.5$; (c) $\lambda/D = 2.8$. Green lines with arrows depict the values of $Re(\epsilon)$ and $Im(\epsilon)$ for various materials (dispersion). The orientation of arrows corresponds to the increase of wavelength from the minimum to the maximum given in microns. [4]

metals, dielectrics support the optical penetration depth much larger than the diameter of the nanoparticle in the visible range. The effective volumes of Mie-type modes are typical of the order of nanoparticle volume $V_{eff} \approx \pi D^3/6$. It means that the increase of the nanoparticle size is effective for the temperature increase in the case of dielectrics and less effective for plasmonic nanoparticles.

1. What parameters determine the value of optical heating of a nanoparticle?
2. What is the difference between pulsed, CW, and quasi-CW regimes for nanoparticles heating?
3. What is the most optimal condition for nanoparticles optical heating?

References

1. Koroteev N. I., Shumai I. L. Physics of intense laser radiation. - 1991.
2. Baffou G. Thermoplasmonics. - Cambridge University Press, 2017. - P. 101-142.
3. Baffou G., Quidant R. Thermo-plasmonics: using metallic nanostructures as nano-sources of heat //Laser & Photonics Reviews. - 2013. - V. 7. - №. 2. - P. 171-187.
4. Zograf G. P. et al. Resonant nonplasmonic nanoparticles for efficient temperature-feedback optical heating //Nano letters. - 2017. - V. 17. - №. 5. - P. 2945-2952.

Макаров Сергей Владимирович
Тигунцева Екатерина Юрьевна
Тонкаев Павел Андреевич

Экспериментальные методы нанофотоники

Учебно-методическое пособие

В авторской редакции
Редакционно-издательский отдел Университета ИТМО
Зав. РИО Н.Ф. Гусарова
Подписано к печати
Заказ №
Тираж
Отпечатано на ризографе

Редакционно-издательский отдел
Университета ИТМО
197101, Санкт-Петербург, Кронверкский пр., 49, литер А